UNIVERSITY OF COPENHAGEN

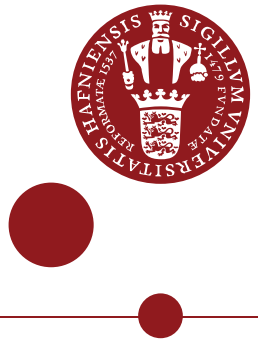

MSc in Climate Change

From South to North: Linking the Southern Ocean Winds to the North Atlantic Deep Convection

Chayton Bouwmeester

Supervised by Markus Jochum

May 2024

Chayton Bouwmeester

From South to North: Linking the Southern Ocean Winds to the North Atlantic Deep Convection

MSc in Climate Change, May 2024

Supervisor: Markus Jochum

University of Copenhagen

Niels Bohr Institute

Blegdamsvej 17

2100 Copenhagen

Abstract

The strong westerly winds in the latitudes of the Southern Ocean have been suggested as a potential driving mechanism for the Atlantic Meridional Overturning Circulation (AMOC). For the winds in the Southern Ocean to influence changes in the North Atlantic, there must be some mechanism that carries information meridionally. In this thesis the ocean model VEROS is used at a 1° resolution with an idealised Atlantic basin to perform two experiments, $\tau_x^{+50\%}$ and $\tau_x^{-50\%}$, where the amplitude of the winds in the latitudes of a periodic channel are increased or decreased by 50% respectively. It is found that a combination of Kelvin-like boundary waves and Rossby waves carries the signal to the North Atlantic, where they enhance or reduce the North Atlantic deep convection via an increase in the mixed layer depth. Analysis of the resulting upwelling structure reveals that stronger winds in the Southern Ocean lead to greater upwelling in the periodic channel, and less in the ocean interior. These results point towards an adjustment process originating in the Southern Ocean, where the increase in the surface Ekman transport results in a greater along-isopycnal upwelling in the ACC, and reduced diapycnal upwelling in the ocean interior.

Contents

1 Background and Theory

1.1 Introduction

The Atlantic Meridional Overturning Circulation (AMOC), is the Atlantic arm of the Global Meridional Overturning Circulation (GMOC), which describes the general pattern of localised deep water formation and upwelling elsewhere (Vallis, 2017, p.801). The AMOC has a strong impact on climate, particularly for that of the North Atlantic. The Gulf Stream is one component of the AMOC which brings warm surface waters from the equator towards Western Europe and results in a relatively mild climate compared to other regions at the same latitudes. Changes in the strength of the AMOC have been implicated in rapid climate change events in the past (Alley *et al.*, 2003) making vital to understand the processes which drive it, and how it responds to forcings if we wish to predict future climate change.

The question of which driving forces are most important in determining the strength of the AMOC is still a subject of inquiry (Kuhlbrodt *et al.*, 2007). The traditional view of the AMOC is that it is primarily driven by meridional differences in buoyancy, which has resulted in it often being referred to as the thermohaline circulation (THC). However, it has also been suggested that winds in the Southern Ocean could instead determine the strength of the overturning (Toggweiler and Samuels, 1995). With the Southern Ocean westerlies having strengthened over the last 50 years (Toggweiler, 2009), and the expectation according to models that this trend will continue in the future (Deng *et al.*, 2022), it is important to understand this connection. The modern view of the AMOC is that it is likely driven by a combination of buoyancy forcing, wind forcing, and diapycnal diffusion (Kuhlbrodt *et al.*, 2007), and therefore the driver-agnostic terms 'AMOC' and 'MOC' as opposed to THC will be preferred.

It is this wind-driven component of the AMOC that is the subject of this thesis. In particular, the issue of how changes in the Southern Ocean winds are

communicated throughout the Atlantic Ocean, and how the AMOC adjusts in response. It is well understood that waves can communicate signals throughout an ocean basin, and establish large scale flow patterns in their wake (Kawase, 1987, Wajsowicz and Gill, 1986, Wajsowicz, 1986). Such waves have been invoked to explain this potential connection in the past (McDermott, 1996), but what is less explored is how exactly these waves result in a change in the overall strength of the overturning. In this thesis, I will use a primitive equation ocean model of an idealised Atlantic basin to investigate this adjustment process.

The primary questions I wish to address in my thesis are:

- Do the Southern Ocean winds influence the strength of the AMOC?
- How are changes in the Southern Ocean wind stress communicated throughout the Atlantic?
- What mechanisms drive the strengthening/weakening of the AMOC?
- How is the resulting upwelling/downwelling structured?

I will begin with outlining some relevant theory and background with regards to the driving processes of the AMOC and how wind forcings are communicated throughout the ocean. In the methods section I will explain the model and experiments I will use to investigate these questions. I will then present the outcome of these experiments in the results, and finally summarise and put them into context in the discussion.

1.2 The Wind Driven AMOC

The traditional view of the AMOC is that of a large scale circulation driven by meridional differences in buoyancy. In essence, water that is lighter than its surroundings will rise, and water that is heavier than its surroundings will sink. One can perhaps see from these basic principles how a circulation could form in a body of water that is warmer at one end and cooler at the other. Perhaps the most illustrative model for the thermohaline circulation is the two-box model from Stommel (1961). Here, two well-mixed reservoirs are connected via an overflow at the surface, and a capillary at depth (Figure 1.1). Each of the reservoirs is also in contact with a source of heat and salinity which result in the two reservoirs having their own densities. The rate of the flow between these reservoirs is then simply proportional to the difference in the density of the water. Interpreting this in the context of the real ocean, the two boxes could be thought of as representing the low and high latitudes of the North Atlantic. We would expect the water in the low latitudes (vessel 1) to be warmer and saltier than the water at the high latitudes (vessel 2). Here in the box model, you therefore have a steady, salinity circulation with movement from vessel 1 to vessel 2 in the overflow, and movement from vessel 2 to vessel 1 in the capillary. Despite the simplifications, the two-box model roughly corresponds to the structure observed in the northern cell of the real AMOC.

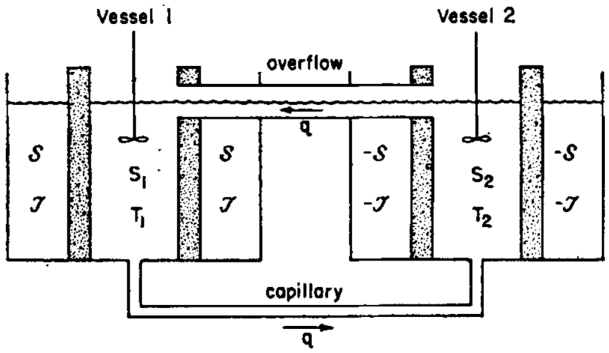

Figure 1.1: Diagram of the Stommel box model, which demonstrates a buoyancy driven circulation. Figure from Stommel (1961).

One significant simplification of the Stommel box model is that the boxes are mixed by a mechanical stirring device such that they both have a uniform density. This is not quite so simple in the real ocean, as both heating and cooling largely occurs at the surface, and for there to exist a deep circulation,

this energy needs to somehow be moved down into the deeper layers. In the absence of a large stirring device in the ocean, there are two mechanisms that could facilitate this downward transport of heat; molecular diffusion and turbulent mixing. However, in a system where the diffusion of heat through the surface is the only forcing, the resulting flow is non-turbulent, clearly unlike the real ocean (Vallis, 2017, p.812). Furthermore, in the real ocean the amount of energy that can be provided through molecular diffusion has been estimated to be at least 10,000 times smaller than the energy available from wind and tidal sources. This means that although it is true that the ocean can in essence function like a heat engine just from thermal forcing at the surface, any potential resultant circulation would be insignificant compared to the mechanically driven component of the MOC (Wang and Huang, 2005).

A series of papers by Stommel, Arons and Faller (1958), and Stommel and Arons (1959a, 1959b), provide the basis for much of the modern theory on abyssal circulation. Driven by laboratory experiments using a rotating tank, they presented a model of the abyssal circulation characterised by a slow uniform upwelling of abyssal waters over large areas of the ocean. This upwelling occurs through diapycnal mixing (mixing across layers of equal density), and rises up from the abyss into the warmer upper layers. This mixing does of course also require a source of energy, which is most often identified as the breaking of internal by the breaking of wind and tidal driven internal waves (Munk and Wunsch, 1998; St. Laurent and Garrett, 2002). There are certain problems that have been found with this theory however. For instance, diapycnal mixing rates have been found to be rather non-uniform, likely owing to variation in bottom topography. This was anticipated by Stommel and Arons at the time, who did recognise that the introduction of bottom topography would result deviations from their theories. Another problem is that observations of the diapycnal mixing into the thermocline indicate that it alone is not sufficient to explain all of the upwelling that should theoretically occur (Ledwell *et al.*, 2011; Toole *et al.*, 1994; Kunze *et al.*, 2006). Therefore, some other pathway may be required to explain the upwelling of abyssal waters.

The idea of a wind-driven AMOC was first presented by Toggweiler and Samuels (1995) and stood in contrast to the prevailing thermohaline driven understanding of the AMOC at the time. Their model of the overturning sidesteps the issue of the diapycnal mixing by instead implicating the upward movement

of water *along* isopycnals that rise in the Antarcic Circumpolar Current (ACC). They proposed that the winds in the latitudes of the Drake Passage were the primary factor determining the strength of the AMOC, which they referred to as the 'Drake Passage effect'. The theory is predicated on the unique dynamical conditions found in the latitudes of Drake Passage, being that it is the only region in the ocean where there are no meridional boundaries down to a depth of approximately 2500 metres. This means that the zonally averaged east-west pressure gradient in this region must be equal to zero and therefore that there can be no net geostrophic meridional flow. Any meridional flow must instead be ageostrophic, and one way in which an ageostrophic meridional flow can be induced is through a surface wind stress (Kuhlbrodt *et al.*, 2007). In the ACC, this northward ageostrophic movement of water comes from Ekman transport. Around Antarctica there are strong westerly winds which act on the surface and through frictional interactions drive movement in a region below the surface called the Ekman layer. Within this Ekman layer, the friction resulting from the surface wind stress is deflected due to the Coriolis force. If integrated across the entire depth of the Ekman layer, the result is a net transport in a direction 90° from the direction of the wind (Figure 1.2). This net flow normal to the direction of the winds is known is Ekman transport. In the Southern hemisphere, this means that the westerly winds in the Southern Ocean induce an equatorward Ekman transport, as the Coriolis force deflects to the left.

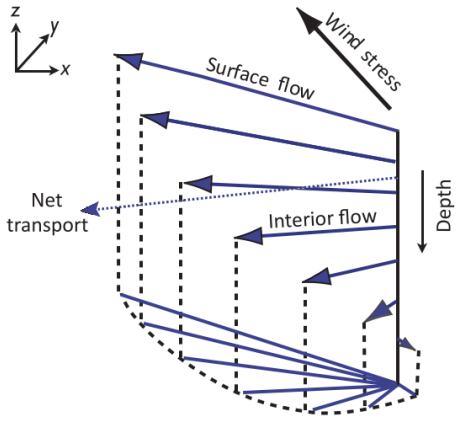

Figure 1.2: Diagram of an Ekman spiral, illustrating the deflection of the frictional stresses due to the Coriolis force. Figure from Vallis, 2017.

This has implications for the AMOC, as this Ekman transport results in an area of divergence south of the wind stress maximum. This pulls deeper water to the surface through a process called Ekman suction. This deep water

must then be replaced by a poleward geostrophic return flow, and due to the presence of the Drake Passage, this can only occur in depths below the depth of the shallowest sill, where meridional boundaries exist, thus creating a deep circulation. This forces the conversion of the dense deeper waters into lighter surface waters. Of course, with this conversion occurring in the ACC, there must be somewhere where the surface waters are then converted to deep water. They identify the only place that this can occur is the convective regions of the North Atlantic, implying that the NADW formation process simply closes this loop created by the dynamics in the Drake Passage. Therefore according to this model, it is the strength of the Southern Ocean winds that is the primary factor determining the strength of the AMOC, through the change in surface Ekman transport. Toggweiler and Samuels tested this hypothesis using a stratified ocean GCM with idealised topography. They observed that there was in fact a strong, linear sensitivity of the AMOC to the strength of the winds in the Southern Ocean.

However, there is also evidence contrary to the Drake Passage hypothesis. More recent model experiments do not show such a strong sensitivity of AMOC intensity to Southern Ocean winds, and suggest that the almost one-to-one relationship found in Toggweiler and Samuels (1995) was unrealistic. The sensitivity largely seems to depend on the representation of baroclinic mesoscale eddies in the particular model used (Gent, 2016). Increasing the wind stress acts to increase the northward Ekman transport as previously discussed, however it also increases the production of these mesoscale eddies. Such eddies have been hypothesised to dampen the effect of the Southern Ocean winds on the strength of the AMOC, as they produce a circulation of opposite sign to the equatorward Ekman transport and deep poleward return flow. This effect is known as eddy compensation. The model used Toggweiler and Samuels (1995) did not account for this eddy compensation effect in their model, meaning the effect could be overestimated. Eddy resolving models consistently show that increasing the strength of the Southern Ocean winds results in an increase in eddy kinetic energy (EKE) in the ACC (Gent, 2016). However the degree to which this eddy compensation occurs varies depending on the model. Some eddy-resolving models, such as that used in Jochum and Eden (2015), find essentially no sensitivity of AMOC strength to Southern Ocean winds. Non-eddy resolving models on the other hand generally show unrealistically large increases in AMOC strength in response to wind changes, as they cannot simulate eddy compensation, however this

effect can be parameterised through a spatially and temporally varying Gent-McWilliams (GM) paramterisation (Gent, 2016).

1.3 Meridional Communication of Wind Forcing in the Atlantic

When there is some forcing applied to the ocean, a physical mechanism is required to transmit this information throughout the ocean to trigger wide-scale adjustment. There are two main mechanisms that have been proposed to explain how buoyancy anomalies can be communicated meridionally in the Atlantic; slowly by advection, or quickly through boundary waves. The relative importance of these two mechanisms seems to be highly model dependant, with studies finding very different propagation time scales for the adjustment of the MOC (Buckley and Marshall, 2016). However, in the specific case of a forcing in the Southern Ocean wind stress, it is primarily waves that have been implicated in previous studies (McDermott, 1996; Webb *et al.*, 2021).

Kawase (1987) demonstrated this wave adjustment mechanism in a two-layer baroclinic model of an idealised Atlantic basin. Here, a buoyancy perturbation originating in the north-west of the model domain results in a Kelvin wave, which travels along coastlines and the equator, establishing boundary currents its wake. These boundary currents then emit westward propagating Rossby waves, which can then communicate the signal into the ocean interior (Figure 1.3). Although this framework was used to demonstrate the 'spin-up' process using a source of deep water at the north-western boundary, such waves can also provide a means of connecting areas of NADW formation to changes in Southern Ocean winds.

The original paper that inspired this thesis was McDermott (1996), who observed this wave adjustment mechanism in the context of the Drake Passage Effect. This study both observes the transient and steady state responses of a stratified ocean model to changes in zonal wind stress in the latitudes of a simulated Drake Passage. In the steady-state case, where winds were applied to an ocean at rest, it was found that the spin-up process proceeded largely as described by Kawase (1987). Boundary waves propagated rapidly along oceanic waveguides, establishing circulation patterns in their wake.

In the transient case, where winds in the latitudes of the Drake Passage were instantaneously increased or decreased in a model that was already in a steady-state, it was observed that Kelvin-like baroclinic downwelling modes were excited, which then also propagated in a similar manner to that which was described in Kawase (1987). These boundary waves travelled first travelled along the south-western coast of the Atlantic, before turning and travelling eastward along the equator, depressing isopycnals in their path. Once reaching the eastern boundary of the Atlantic, the energy being carried by these baroclinic modes divided symmetrically, with half being directed northwards along the east coast of the North Atlantic, and the rest being directed southwards along the South Atlantic coast. As the wind forcing was applied to an already equilibrated model, there already existed areas of NADW formation. The modes were then described to "lock on" to these NADW formation sites, where they would then enhance the convection there. How exactly these baroclinic modes actually increase NADW formation upon reaching these sites was not discussed, and is a topic I aim to expand upon in this thesis.

This adjustment process has also been investigated before in Webb et al. (2021), which I will regularly refer to as a point of comparison. In this study, they use a high resolution global ocean model to investigate the communication of anomalies resulting from a wind stress forcing. They performed two wind forcing experiments. In the first they increased the strength of the winds in the Southern Ocean by 15% (henceforth $\tau^{+15\%}$), and in the second they also increased the winds by 15% but also uniformly shifted the winds 4° southwards (henceforth $\tau^{+15\%}_{4^\circ S}$). As in previous studies, they also identified rapidly propagating boundary waves and more slowly propagating Rossby waves as the primary mechanisms responsible for the adjustment of the AMOC. They expand on previous work by also identifying how the signal enhances the overturning once it reaches the convective regions in the North Atlantic. In their $\tau^{+15\%}_{4^\circ S}$, they identify that the arrival of the signal in the north coincides with a deepening of the mixed layer, and that this increase vertical mixing is what strengthens the AMOC. The overturning response in this case originates in the north, and then migrates southwards. In the $\tau^{+15\%}$ case, they also identify such a response in the mixed layer, but it is much weaker than $\tau^{+15\%}_{4^\circ S}$ case, and instead find that the anomalous overturning largely originates in the forcing region and migrates northward. Webb et al. (2021) do not place such a

large emphasis on this response in the South Atlantic in the $\tau^{+15\%}$ experiment, and therefore I will also attempt to address this.

Often when analysing the output of ocean models, different kinds of waves are distinguished through where, and on what time scales anomalies propagate. However, Marshall and Johnson (2013) point out that this can be misleading, as the amplitude of waves can change as they propagate, which complicates the measurement of phase speeds. Furthermore, different kinds of waves can coincidentally have similar speeds and propagation pathways. They suggest that Kelvin waves are actually unimportant in the adjustment process for periods longer than just a few months. Instead this occurs through a combination of short and long Rossby waves. These short Rossby waves also coincidentally travel speeds to first-mode baroclinic Kelvin waves, and are also boundary-trapped, as Kelvin waves are. To acknowledge this uncertainty, for the purposes of this thesis I will largely refer to these Kelvin-like modes as boundary waves.

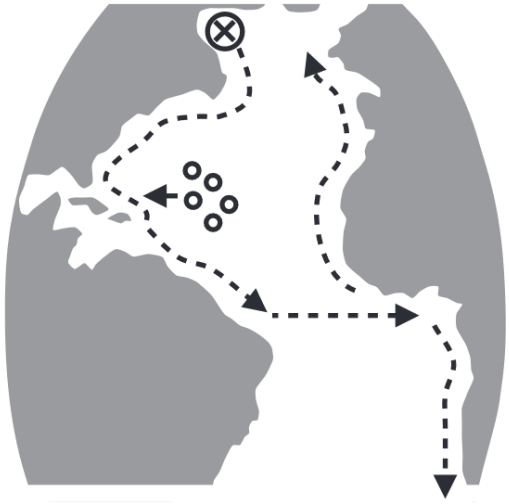

Figure 1.3: Diagram of the boundary wave adjustment process described by Kawase (1987). Boundary waves (dashed arrows) and Rossby waves (rings) adjust the MOC in response to localised forcing (downward arrow). Figure from Marshall and Johnson, 2013.

Overall these studies show two distinct responses in the overall AMOC adjustment process. The Webb et al. (2021) $\tau^{+15\%}_{4^\circ S}$ experiment, and McDermott (1996) implicate changing dynamics in the Northern convective regions as the primary process the causes structural changes in the AMOC. On the other hand, the process described in Toggweiler and Samuels (1995) implies that although there are indeed changes in the northern convective regions, this

process only acts to close the circulation, and shows that the anomalous overturning originates largely in the southern forcing region, due to changes in the surface Ekman transport. This response originating in the south is also seen in the The Webb et al. (2021) $\tau^{+15\%}$ experiment. It is of course also possible that both of these processes play a role, in which case an anomaly could be observed coming from both the north and the south. This is another aspect of the adjustment process I will explore in the results.

1.4 Waves

As previously mentioned, waves are an important mechanism that are often implicated in the adjustment of the ocean to a forcing. In this thesis, I will be primarily concerned with two types of waves involved in this process; Kelvin waves and Rossby waves.

1.4.1 Kelvin Waves

Kelvin waves are a type of gravity wave which arise from the balance between topographic boundaries and the Coriolis force. Although it was briefly mentioned before that Kelvin waves may not so important for the adjustment of the ocean, the alternative short Rossby waves propagate similarly, and Kelvin waves are still a useful example for illustrating the properties of these kinds of boundary waves.

One can imagine situation where a perturbation results in water piled up against a east-west boundary. Due to gravity, this creates a pressure gradient force pointed normal to the boundary. This pressure gradient force must be balanced by the Coriolis force, acting in the opposite direction, which in this case is towards the boundary. As the Coriolis force acts to the right of a current in the Northern Hemisphere, this means we have a current travelling eastwards along this boundary. Conversely, a dip against the wall would result in a pressure gradient forces pointed towards the wall, and therefore the Coriolis would point away, and therefore the current is moving westwards. This back and forth motion against propagates along the boundary like a gravity wave. These are Kelvin waves.

Mathematically, they are wave-like solutions of the linearised shallow-water equations when the assumption of a solid lateral boundary is added. This derivation largely follows that shown in Vallis (2017, pp.126-127). Starting from the the linearised shallow-water equations:

$$\frac{\partial u'}{\partial t} - f_0 v' = -g\frac{\partial \eta'}{\partial x}, \tag{1.1}$$

$$\frac{\partial v'}{\partial t} + f_0 u' = -g\frac{\partial \eta'}{\partial y}, \tag{1.2}$$

$$\frac{\partial \eta'}{\partial t} + H\left(\frac{\partial u'}{\partial x} + \frac{\partial v'}{\partial y}\right) = 0. \tag{1.3}$$

Then, if we assume a boundary at $y = 0$ we can set v' to zero, representing the boundary with the no-normal flow boundary condition. The equations then become:

$$\frac{\partial u'}{\partial t} = -g\frac{\partial \eta'}{\partial x}, \tag{1.4}$$

$$f_0 u' = -g\frac{\partial \eta'}{\partial y}, \tag{1.5}$$

$$\frac{\partial \eta'}{\partial t} + H(\frac{\partial u'}{\partial x}) = 0. \tag{1.6}$$

Combining the zonal momentum equation (1.4) and the continuity equation (1.6) gives the standard wave equation:

$$\frac{\partial^2 u'}{\partial t^2} = c^2\frac{\partial^2 u'}{\partial x^2}, \tag{1.7}$$

Where c is the phase speed of shallow water waves, given by:

$$c = \sqrt{gH} \tag{1.8}$$

Where H is the depth of the fluid. From $c = \omega/k$, we also get a dispersion relation of:

$$\omega = k\sqrt{gH} \tag{1.9}$$

Taking the phase speed equation (1.8), the predicted phase speed for a 4000 metre deep ocean is therefore about $200m/s$. This is very fast, but this is also just the speed for surface, also known as barotropic, Kelvin waves. Most often implicated in basin-wide adjustment to forcings are instead baroclinic or internal Kelvin waves. These kinds of Kelvin waves instead propagate along the interface between isopycnals, at a speed that is instead dependant on the reduced gravity g', while H becomes the equivalent depth for the given baroclinic mode. This means that typical phase speeds of internal Kelvin waves are typically more on the order of 1-3m/s. Another feature of Kelvin waves is that they are non-dispersive, meaning that the phase speed does not depend on the wavenumber. The group speed, c_g, is defined as:

$$c_g = \frac{\delta\omega}{\delta k} \tag{1.10}$$

Applying this to the dispersion relation (equation (1.9)):

$$c_g = \frac{\delta}{\delta k}(k\sqrt{gH}) = \sqrt{gH} \tag{1.11}$$

Which is just the same as the phase speed. The group speed is the speed at which the wave carries information, which means for Kelvin waves, they carry information at the same speed and direction as the phase.

Another important property of Kelvin waves is that they decay exponentially away from the boundary. This can be seen by solving 1.7, which yields the following solution for the surface height:

$$\eta' = \sqrt{\frac{H}{g}}e^{-y/L_d}G(x-ct) \tag{1.12}$$

And the following for the zonal velocity:

$$u' = e^{-y/L_d}G(x-ct) \tag{1.13}$$

Where G is a function representing the wave profile, and L_d is known as the Rossby radius of deformation. The Rossby radius of deformation refers to the fact that the Coriolis force becomes stronger with latitude, and is defined as the length scale at which the influence of the Coriolis force becomes just as important as the effects of buoyancy or gravity, i.e.

$$L_d = \frac{\sqrt{gH}}{f} \tag{1.14}$$

These equations reveal a characteristic property of Kelvin waves, in that we can see from the exponential term that the wave decays rapidly away from the boundary. Similar solutions can be found for other boundaries in the ocean, where in the Northern Hemisphere, the boundary is always on the right of the wave propagation, and in the Southern Hemisphere it is on the left. The equator can also act as a boundary due to the changing of the sign of the Coriolis force, and therefore supports the propagation of equatorial Kelvin waves.

1.4.2 Rossby Waves

As seen in the previous section, Kelvin waves have their maximum amplitude at the boundary and decay exponentially as distance to the boundary increases. Therefore, they cannot be responsible for communicating changes to the interior of the ocean. However, Rossby waves can radiate out from Kelvin waves as they propagate, carrying information into the ocean's interior. Rossby waves are large-scale waves generated by the Earth's rotation and variation in the Coriolis effect with latitude. They also play a crucial role in the communication of signals across the ocean basins. They arise from the fact that the planetary vorticity, also known as the Coriolis force, varies in latitude, and that the potential vorticity is a conserved property in the absence of friction or direct forcing. The potential vorticity is defined as:

$$q = \frac{f + \zeta}{H} \tag{1.15}$$

Where H is again either the equivalent depth of a given mode in a baroclinic fluid, or the depth of the whole fluid in barotropic conditions. f is the planetary vorticity, given by:

$$f = 2\Omega sin\theta \tag{1.16}$$

And ζ is the relative vorticity, which refers to the vorticity of a parcel of water relative to the the Earth's surface. It is given by:

$$\zeta = \frac{\delta v}{\delta x} - \frac{\delta u}{\delta y} \tag{1.17}$$

Using these simple principles, the propagation of these waves is illustrated in Figure 1.4. If a parcel of water is perturbed poleward, it moves into a region where the planetary vorticity is higher, and to conserve its potential vorticity, it must decrease its relative vorticity, which therefore results in a clockwise rotation. Conversely, if it is perturbed equatorward, it must increase its relative vorticity, resulting in counterclockwise rotation. Together, these processes result in an overall westward propagation of the wave.

Mathematically, Rossby waves travelling in a continuously stratified fluid, like those implicated in oceanic adjustment, can be derived from the linearised quasi-geostrophic potential vorticity equation. Solving this and restricting our view to just the zonal and meridional directions yields the following dispersion relation:

$$\omega = \frac{-\beta k}{\frac{1}{L_d^2} + k^2 + l^2} \tag{1.18}$$

Where l is the meridional wavenumber, k is the zonal wavenumber, and L_d is the Rossby radius of deformation.

Long Rossby waves, which are what we are interested when discussing communication into the ocean interior, are at the limit of small zonal and meridional wavenumbers (small values of k and l). We can then get the phase speed of these waves the same way, with $c = \omega/k$, which simplifies to:

$$c = -\beta L_d^2 \tag{1.19}$$

Which means that the waves travel fastest at the equator, and are slower with increasing latitude. Long Rossby waves, like Kelvin waves, are also non-dispersive. As shown in the case of Kelvin waves, and using the simplified dispersion relation at the limit of low wave numbers, we can see:

$$c_g = \frac{\delta}{\delta k}(-\beta k L_d^2) = -\beta L_d^2 \tag{1.20}$$

Which again is just the same as the phase speed. In the case of internal (baroclinic) Rossby waves, H again becomes the equivalent depth for the given baroclinic mode when calculating the Rossby radius of deformation, and g becomes g' (the reduced gravity). Taking a typical value of 40 kilometres for L_d at 30°N (Chelton *et al.*, 1998) and taking β as 2x10$^{-11}m/s$, we arrive at an estimated phase speed of 3.4cm/s for a long Rossby wave travelling along 30°N, which is considerably slower than the aforementioned Kelvin waves.

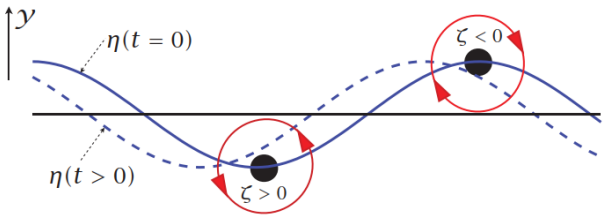

Figure 1.4: Diagram illustrating the propagation of Rossby waves (from Vallis (2017), p.230).

Model Domain and Setup

2

To investigate these topics I used the Versatile Ocean Simulator (Häfner *et al.*, 2018), a primitive equation finite-difference ocean model written in pure Python and based on the pyOM2 model. VEROS uses a three-dimensional Arakawa C grid with free-slip boundary conditions for momentum and no-normal flow boundary conditions for tracers.

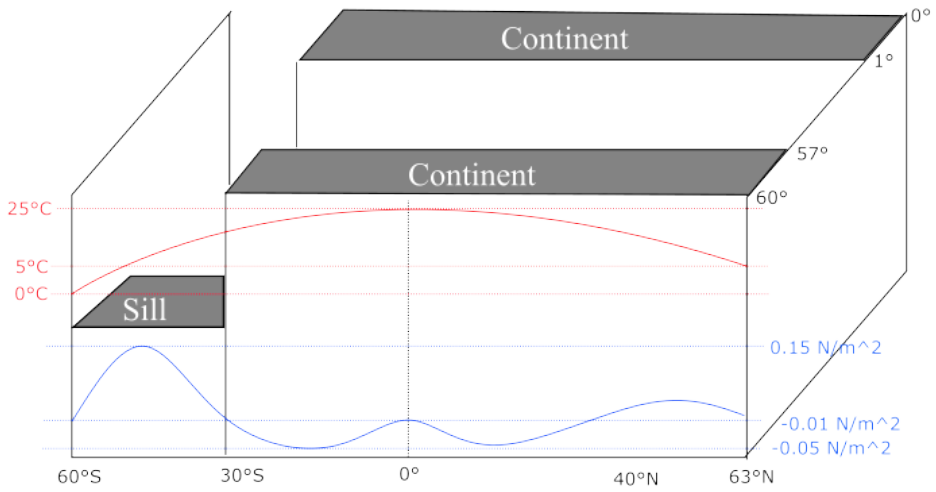

Figure 2.1: Diagram of initial model setup used prior to wind adjustment. Adapted from Hansen (2023) and Andreasen (2020).

The model domain is largely based on that of Hansen (2023), and is an idealised Atlantic Ocean, with 60 degrees of longitude and 124 degrees of latitude (Figure 2.1). The depth is stratified with 50 levels, with a constant maximum depth of 4000 metres. The depth layers use a Vinkour grid, refined towards the surface. Lateral boundaries, representing the continents, create no-normal flow boundary conditions except for latitudes below -30°S, where a re-entrant channel of 2000 metre depth is created to simulate the effects of the Drake Passage.

A sinusoidal wind profile is applied, largely as described in Andreasen (2020), adjusted slightly for the increased size of the model domain (Equation 2.1). Only zonal wind stresses are applied. The temperature forcing is also taken

from Andreasen (2020), where the surface is relaxed to the temperature profile illustrated in Figure 2.1 on a restoring timescale of 10 days. The salinity is restored to a constant background value, also on a timescale of 10 days.

Although as previously discussed that a dynamic EKE parameterisation scheme is necessary to represent the effects of eddy saturation on the overturning strength in non-eddy resolving models, a constant GM coefficient will instead be used. This is because the focus of the study is more on the mechanisms that result in the adjustment of AMOC following the wind forcing, and therefore a relationship between the Southern Ocean winds and the North Atlantic MOC is actually desired. However this does mean that the magnitude of the response in the AMOC strength will likely be unrealistic. The various key parameters set for the model are shown in Table 2.1.

$$\tau_x(\theta) = \begin{cases} 1.5 \sin\left(\frac{\pi}{30^\circ}\theta + 60^\circ\right), & \text{if } \theta < -30^\circ \\ -0.05 \sin\left(\frac{\pi}{30^\circ}(\theta - 30^\circ)\right), & \text{if } -30^\circ < \theta < -5^\circ \\ -0.015 \cos\left(\frac{\pi}{10^\circ}(\theta - 10^\circ)\right) - 0.025, & \text{if } -5^\circ < \theta < 5^\circ \\ 0.05 \sin\left(\frac{\pi}{30^\circ}(\theta - 30^\circ)\right), & \text{if } 5^\circ < \theta < 30^\circ \\ -0.5 \sin\left(\frac{\pi}{63^\circ - 30^\circ}\ (\theta - 63^\circ)\right), & \text{if } 30^\circ < \theta \end{cases} \tag{2.1}$$

Key Parameters		
Parameter Name	Value	Units
Lateral Viscosity	2.2e5	m^2/s
Bottom Friction	1e-5	s^{-1}
Gent-McWilliams Parameter	1000	m^2/s
Salinity Restoring Timescale	10	Days
Temperature Restoring Timescale	10	Days
Time Step	3600	Seconds

Table 2.1: Key parameters used in the simulation.

The model is initially spun up for 450 years, after which the the run separates into three branches, being two experiments and a control. In the first experiment (henceforth referred to as $\tau_x^{+50\%}$), the amplitude of the winds in the latitudes of the simulated Drake Passage (below -30°S) are instantaneously increased by 50%. In the second experiment they are instantaneously reduced by 50% (henceforth referred to as $\tau_x^{-50\%}$) (Figure 2.2). The rest of the model parameters are left unchanged. After branching off, the models are run for

a further 50 years, however due to storage limitations, the first 15 years are computed as daily averages whereas subsequent years are yearly averages. The daily data will be used primarily for investigating the signal propagation, whereas the annual averages will be used for analysing longer term adjustment to the wind forcing.

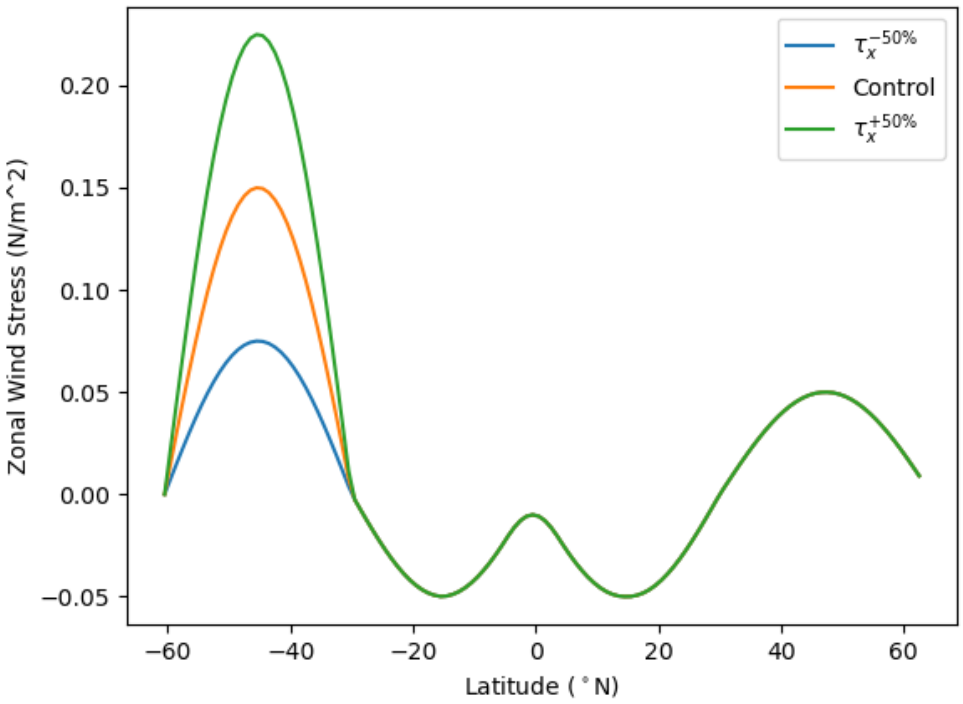

Figure 2.2: Wind profiles for the 3 experiments. The wind stress is only adjusted for the latitudes of the simulated Drake Passage. $\tau_x^{-50\%}$ is shown in blue, $\tau_x^{+50\%}$ in green, and the control in orange.

3 Results

In this section I will present the results of the model experiments. The results are divided to 5 subsections, each addressing a different aspect of the overturning response. I will begin by presenting the AMOC at the end of the spinup period. I will then confirm any sensitivity between the AMOC and the wind stress. After seeing there is a sensitivity, I will describe the signals produced following the wind forcing. These signals induce changes in the mixed layer depth, which will be then be presented. Finally, I will describe the overall resulting upwelling structure from the experiments.

3.1 Spinup

The model is initially spun up for 450 years, after which the zonally averaged overturning streamfunction is as shown in Figure 3.1. The overturning structure looks largely as expected, with an upper cell, associated with the North Atlantic Deep Water (NADW) formation, and a lower cell, originating from the Antarctic Bottom Water formation. The upper cell shows sinking at the high northern latitudes to a depth of about 2000 metres, after the which the water is broadly upwelled area across the Atlantic. The bottom cell contains the densest water, originating at the southern boundary and fills the abyss. The directly wind-driven deacon cell is also present at about 30-60°S, with sinking at the northern end due to the Ekman pumping, and upwelling at the southern end from the Ekman suction. The strongest circulation of the deacon cell is occurring down to around 2000 metres depth, corresponding to the depth of the re-entrant channel.

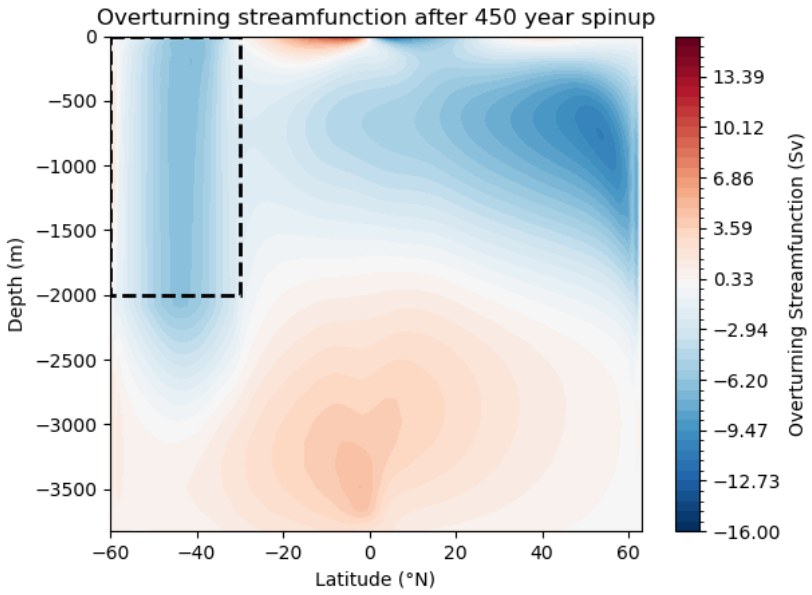

Figure 3.1: Overturning stream function plotted in depth space at the end of the 450 year spinup period. Negative values indicate clockwise circulation, while positive values indicate anti-clockwise circulation. The dashed black box indicates the area of the re-entrant channel.

3.2 AMOC Strength and Southern Ocean Winds

Using the model setup described in Chapter 2, I adjusted the strength of the winds in the Southern Ocean and observed the effects on the overturning strength. First, we will verify that there is indeed a relationship between the wind stress and the overturning strength in this particular model and setup. As can be seen from Figure 3.2a, there is a clear and fast response in the maximum overturning strength of the upper cell at 40°N following the wind forcing. In $\tau_x^{+50\%}$, the intensity increases steadily in comparison to the control, whereas in $\tau_x^{+50\%}$ it decreases, both as expected. After the 50 year period, the maximum overturning at this point increased by approximately 12.9%. $\tau_x^{-50\%}$ shows essentially the same response in the opposite direction and develops in a similar manner, with a 12.9% decrease in the maximum overturning strength after 50 years. In the Southern Hemisphere measured at 10°S, a much larger sensitivity is shown, with a 44.7% intensification in $\tau_x^{+50\%}$ and a 47.2% weakening in $\tau_x^{-50\%}$ (Figure 3.2b). The two experiments also clearly depart from the control earlier in the South Atlantic than in the North

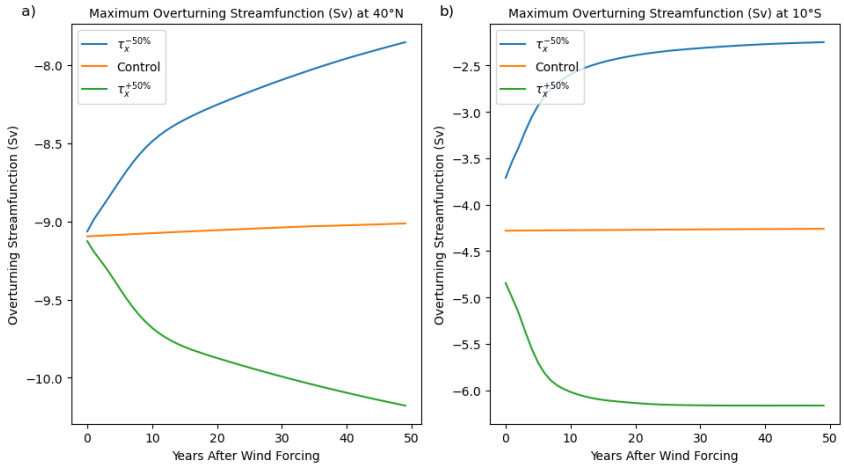

Figure 3.2: Annually averaged maximum overturning stream function of the upper cell over time measured at 40°N and 10°S for the three different experiments ($\tau_x^{-50\%}$ in blue and $\tau_x^{+50\%}$ in green) and the control (orange).

Atlantic. As the data is in yearly averages, the large gaps between the lines at the beginning of the time evolution plots indicates that a significant change is happening within the fist year. The fact that the overturning responds more quickly at these southern latitudes also suggests an adjustment originating from the forcing region.

To more clearly see from where the changes in the AMOC are originating, we can look at the spatial development of the overturning anomaly. The anomaly in the maximum overturning strength expands northwards rapidly from the forcing region until it reaches the equator, after which it continues northwards more slowly (Figure 3.3). Although it takes some years before there is a significant change in the overturning in the north, initial changes in the overturning anomaly reach the northern boundary on timescales of just a few months. This picture of the AMOC, where the response of the Southern Ocean is dominant in influencing the overall overturning strength resembles that of the original study on the topic by Toggweiler and Samuels (1995). If it is the change in the Ekman pumping/suction following a wind forcing that is the dominant process affecting the strength of the AMOC, then it would be expected that the AMOC anomaly would originate south and propagate northwards in this manner. As these figures show the zonally averaged overturning, we cannot yet explore where in the ocean these adjustments are actually occurring, and what is causing them. I will return to this later in the results in Section 3.5.

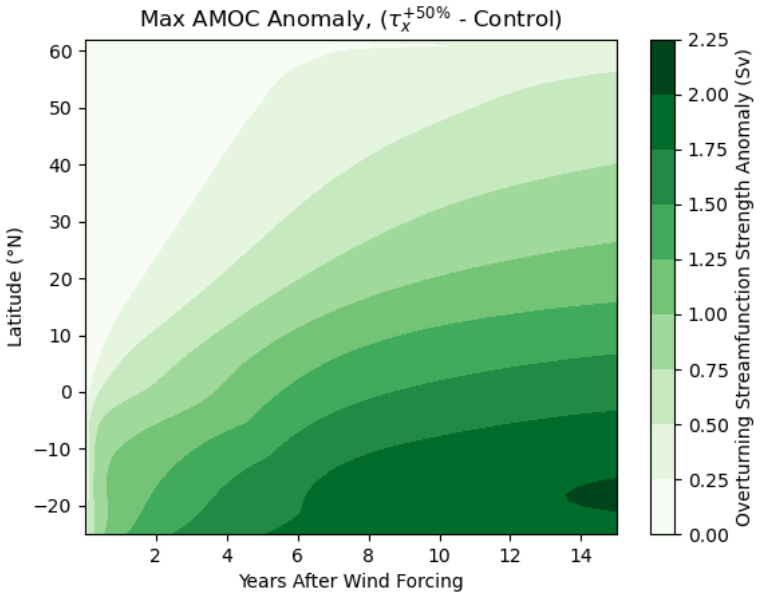

Figure 3.3: Maximum AMOC anomalies for 15 years following the forcing in the $\tau_x^{+50\%}$ experiment.

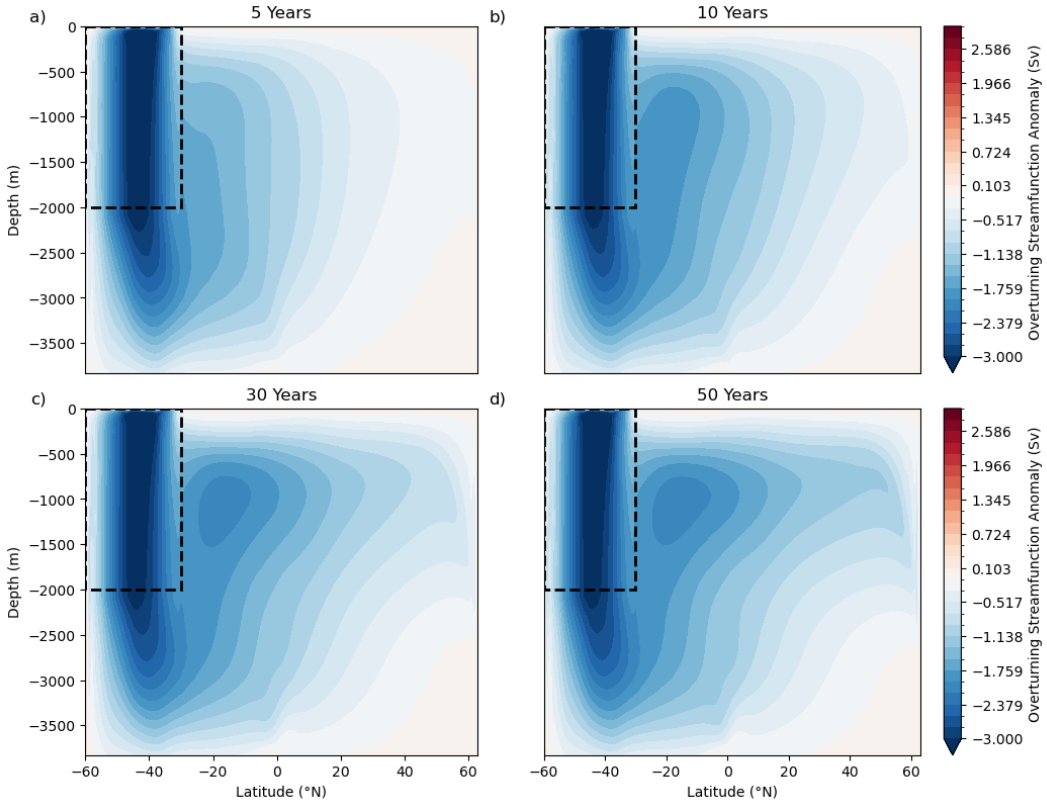

Figure 3.4: Overturning streamfunction anomalies ($\tau_x^{+50\%}$ - Control) after (a) 5 years, (b) 10 years, (c) 30 years, (d) 50 years. The black dashed lines indicate the outline of the re-entrant channel.

3.3 Signal Propagation

As originally suggested by McDermott (1996), Kelvin-like baroclinic modes can follow oceanic waveguides and cross the equator, connecting the Southern Ocean winds and the North Atlantic. In this section, I will also explore this phenomenon, and attempt to identify and measure these signals. The waves should be associated with a signal in pressure, density, velocity, or temperature (Marshall and Johnson, 2013). These variables can be used to track and analyse the nature of the signal generated in these experiments. I will mostly consider the signal at a depth of approximately 200 metres, as the depth of the maximum anomaly is around here.

Immediately after the wind forcing in both $\tau_x^{+50\%}$ and $\tau_x^{-50\%}$, fast moving signals originating from the forcing region can be seen in the density anomaly (Figures 3.5 and 3.6). These signals propagate similarly to Kelvin waves along oceanic waveguides, and proceed largely as described by McDermott (1996) and Kawase (1987). These modes are excited at the south-west boundary of the model domain, just north of the simulated Drake Passage. They proceed to travel northwards along the coastline, and then turn and travel eastward along the equator. Upon reaching the eastern boundary, the signal then splits symmetrically, where it continues along the eastern boundaries towards both the north and south. At the eastern boundaries, some of the energy of these signals is directed westward as Rossby modes, carrying the signal into the ocean interior. The boundary waves arrive at the north-eastern corner of the model domain on timescales of just a few of months (Figure 3.10c). The waves propagate the same way in both the $\tau_x^{+50\%}$ (Figure 3.5) and $\tau_x^{-50\%}$ (Figure 3.6), but simply differ in the sign of the anomaly.

The propagation of these rapid boundary waves changes once it reaches the north-eastern corner. Instead of the maximum of the signal continuing in the upper few hundred metres, it appears to shift downwards to a depth of approximately 2500 metres at the northern boundary (Figure 3.7). This is because of the significant weakening of the stratification that the waves encounter in this region (Figure 3.9a). In the ocean, both the abyss and the mixed layer are weakly stratified. In the convective regions in the north, the mixed layer deepens significantly, as the formation of deep water at this surface sinks and erodes the stratification beneath. This downward shift could

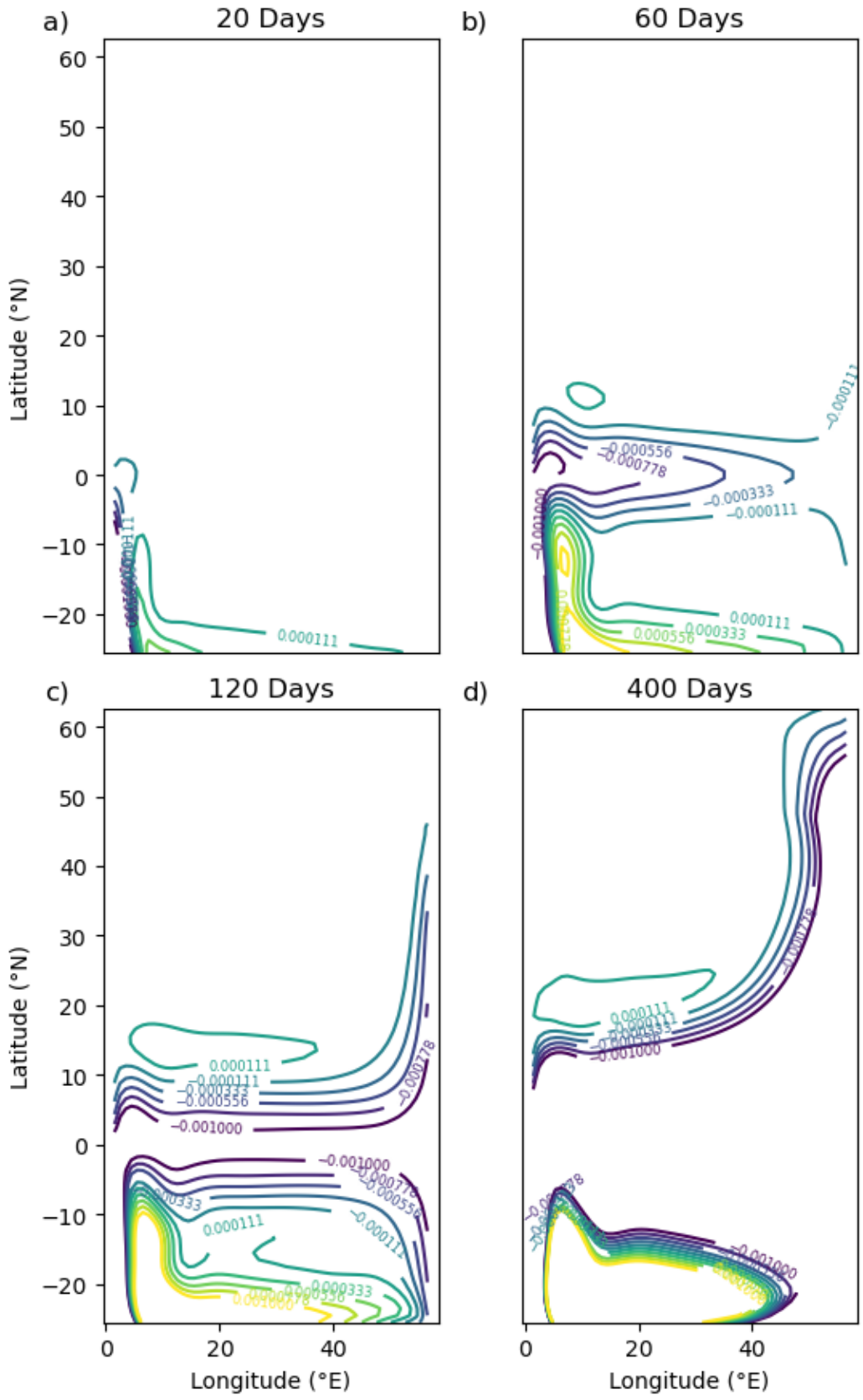

Figure 3.5: Density anomalies ($\tau_x^{+50\%}$ - Control) at 218.7m depth after (a) 20 days, (b) 60 days, (c) 120 days, (d) 400 days.

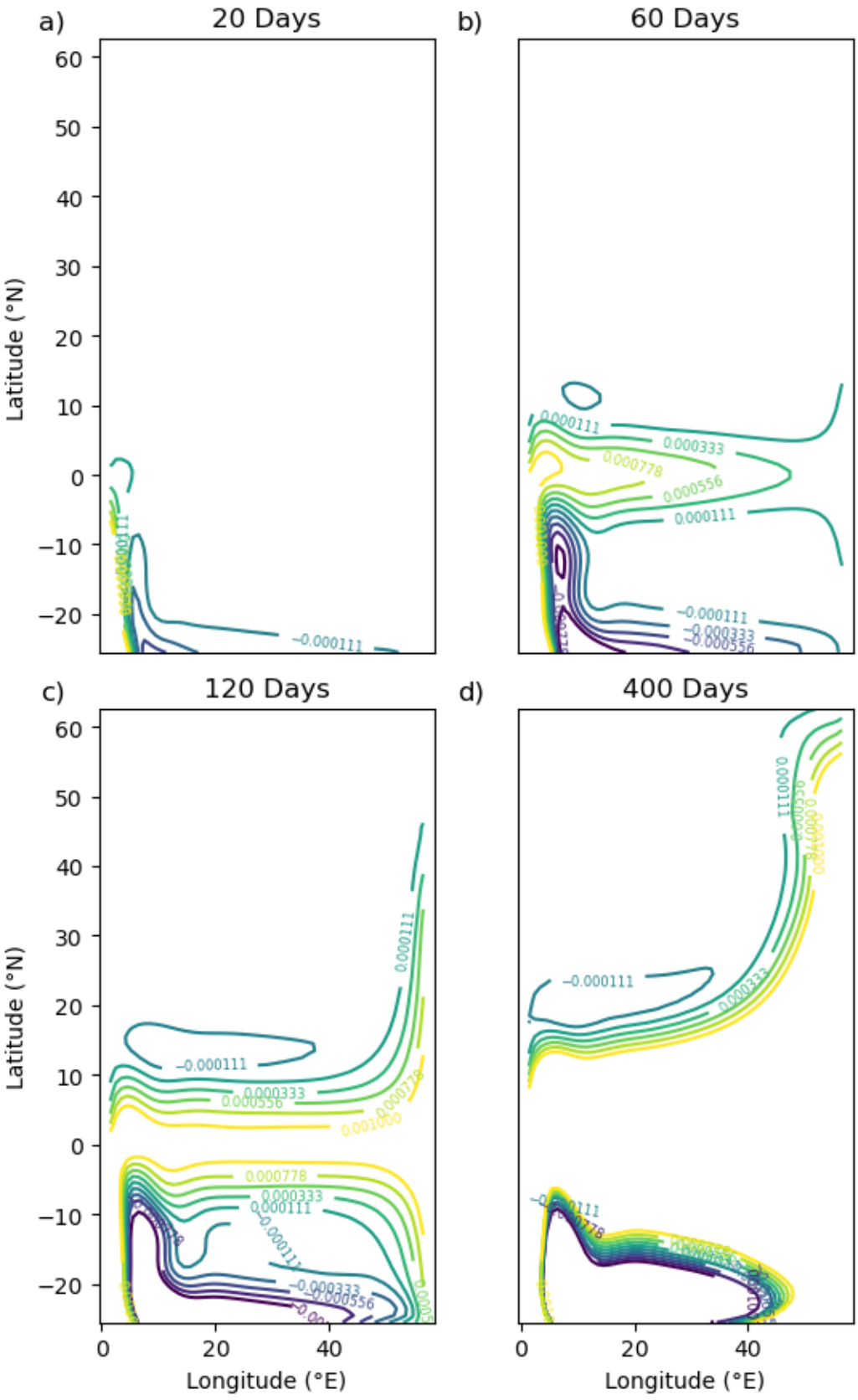

Figure 3.6: Density anomalies ($\tau_x^{-50\%}$ - Control) at 218.7m depth after (a) 20 days, (b) 60 days, (c) 120 days, (d) 400 days.

therefore simply be due to the signal travelling along isopycnals, which change depth significantly in this region. As a result, the strongly stratified pycnocline, where the strongest signal was previously, also occurs at a much lower depth.

Alternatively, this behaviour could be interpreted in terms of the dispersion relation of internal gravity waves, $\omega = Ncos\theta$. When such waves encounter a region of very weak stratification, the waves tend to reflect as they are unable to propagate through a region where the buoyancy frequency is less than the wave frequency ($\omega^2 < N^2$), where the signal then rapidly decays. However, the contours of the buoyancy frequency can also be seen to penetrate downwards, offering a path for the wave where the stratification is again stable enough for it to propagate (Figure 3.9). This region where the N^2 is relatively high compared to its surroundings, but is sandwiched between the weakly stratified abyss and mixed layers where N^2 is very low therefore acts as a waveguide, which forces the wave to propagate deeper. A definitive explanation reasoning behind the wave dynamics in this region, while worthy of further exploration, is beyond the scope of this thesis.

The maximum of the anomaly can be seen to continue following this region of stronger stratification along the northern boundary (Figure 3.8), where it continues on a slight angle downwards following the pattern in buoyancy frequency shown in Figure 3.9d. McDermott (1996) does hint towards changing wave dynamics upon reaching the northern convective regions when discussing the 'lock-on' mechanism, which refers to the tendency of the boundary waves to 'lock on' to pre-existing sinking regions following a wind forcing as the lack of stratification in these regions offer a 'path of least resistance'. However, it is not described that this signal can actually continue along the northern boundary at a a greater depth.

The phase speeds of these waves can be estimated by taking the slope of a Hovmöller diagram. This is somewhat problematic as Marshall and Johnson (2013) point out that the amplitude of a wave need not remain constant as it travels along boundaries. This means that there are uncertainties with using this rather crude method to measure phase speeds, however it will suffice for illustrating the order of magnitude of the waves speeds. In the case of the boundary waves, the phase speeds are estimated to be on the order of 1 m s^{-1}, although the exact estimate varies slightly depending on the depth and the precise contour being measured (Figure 3.10). This is consistent

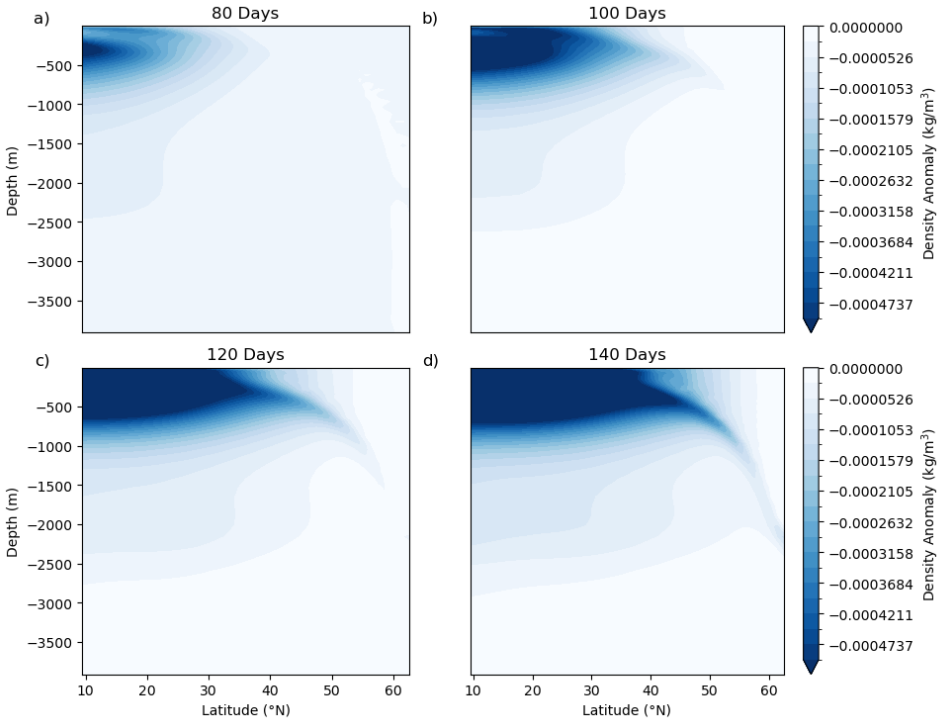

Figure 3.7: Density anomalies ($\tau_x^{+50\%}$ - Control) along the eastern boundary (56.5°E) after (a) 80 days, (b) 100 days, (c) 120 days, (d) 140 days.

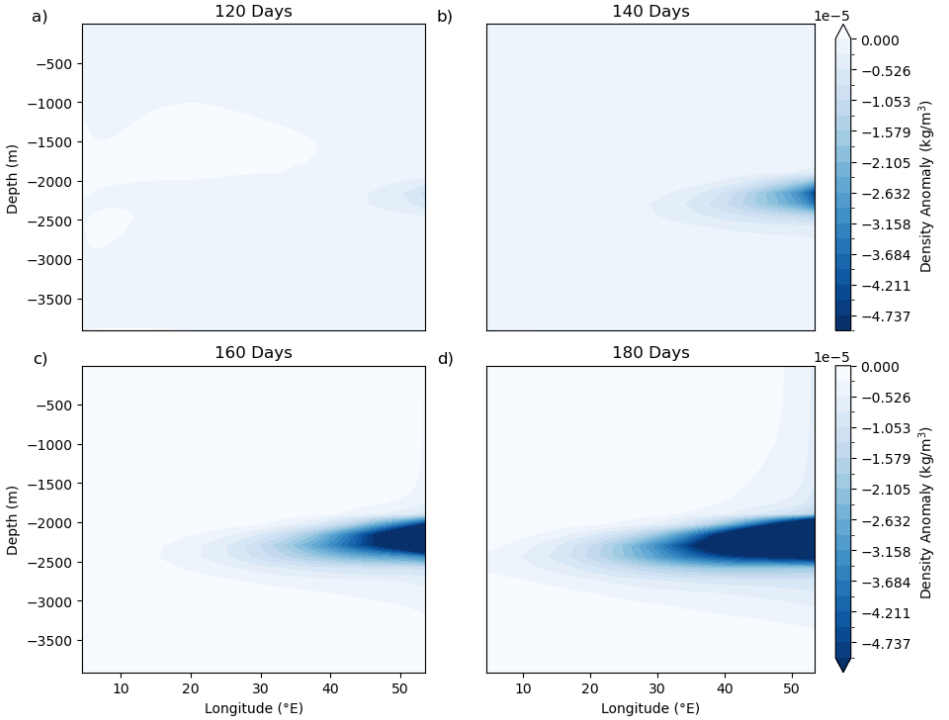

Figure 3.8: Density anomalies ($\tau_x^{+50\%}$ - Control) along the northern boundary (62.5°N) after (a) 120 days, (b) 140 days, (c) 160 days, (d) 180 days.

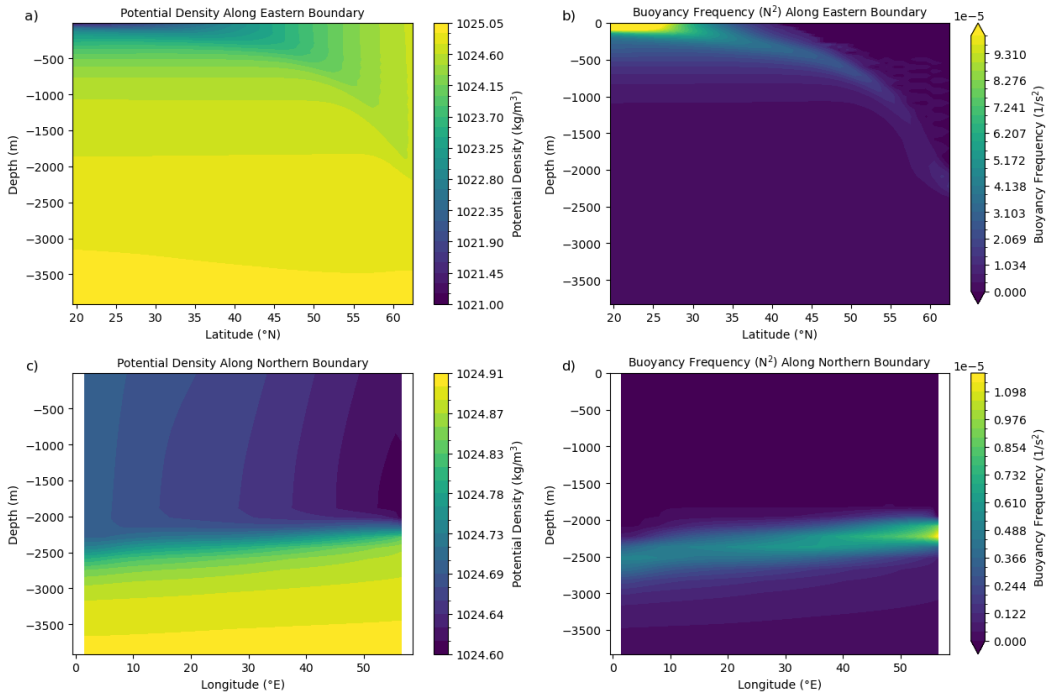

Figure 3.9: Potential density and buoyancy frequency at the eastern boundary ((a) and (b) respectively) and northern boundary ((c) and (d)). Values are from the end of the spinup period.

with first-mode baroclinic boundary waves, and consistent with the speeds found in McDermott (1996) and Webb et al. (2021). The slower moving waves propagating into the ocean interior travel much slower, at speeds of approximately 5 cm s^{-1} (Figure 3.11). These speeds are typical of long Rossby waves in the mid-latitudes of the North Atlantic (Osychny and Cornillon, 2004). The Rossby waves at higher latitude also appear to be propagating slower than at lower latitudes, which matches theoretical expectations due to the change in the Rossby radius of deformation (equation 1.19).

According to Marshall and Johnson (2013), the speed of the boundary waves should be dependant on the Rossby radius of deformation, which decreases poleward. This should be reflected in by a change in the speed of the northward propagating boundary waves, however this is not clear from these plots (Figure 3.10a and c). Furthermore, stratification can also affect the phase speed of coastal Kelvin waves, where a weaker stratification results in a reduced speed (Greatbatch and Peterson, 1996), which could alternatively explain any change in speed. To be able to properly diagnose these waves would likely require more experiments adjusting the boundary layer width and the resolution to determine whether these waves are classical Kelvin waves, or

if they are short/long Rossby waves as suggested by Marshall and Johnson, 2013. Therefore, they will simply be referred to as boundary waves.

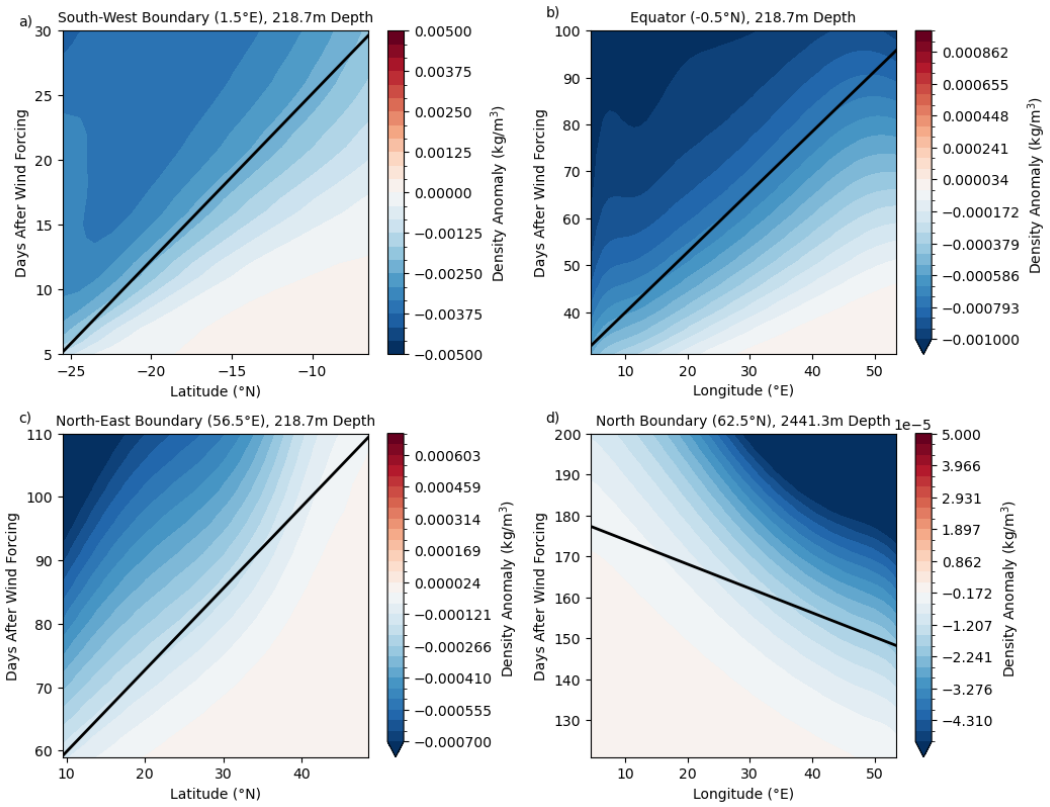

Figure 3.10: Hovmöller diagrams of the density anomalies along different oceanic waveguides in $\tau_x^{+50\%}$. The plots shown are for the south-western boundary (a), the equator (b), the north-eastern boundary (c), and the northern boundary (d). The black lines indicate a speed of 1 m s^{-1}.

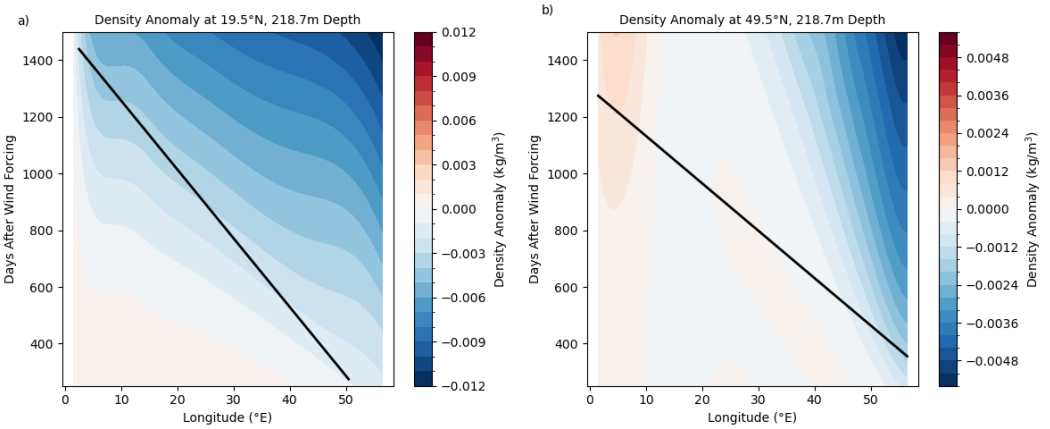

Figure 3.11: Propagation of the density anomaly in $\tau_x^{+50\%}$ into the ocean interior across 29.5°N (a) latitude and 49.5°N (b) at 218.7 metre depth. The black lines indicate a speed of 5 cm s^{-1}.

As previously indicated, the boundary waves generated in $\tau_x^{+50\%}$ are associated with a negative density anomaly implying that it is propagating as a downwelling wave, which depresses isopycnals in its path. This can be seen in Figure 3.5, where a constant depth is shown, and therefore a negative density anomaly implies an downwelling of the lighter surface layers. In $\tau_x^{-50\%}$, an upwelling signal is instead observed, where denser, deeper layers are brought up to the depth being measured. The resultant long Rossby waves from the north-eastern boundary are also downwelling waves in the $\tau_x^{+50\%}$ experiment. This is consistent with the pattern described in Webb et al. (2021), where it is described that the relative location of the wind stress curl to the lateral boundaries determines the sign of the signal. Increasing the amplitude of the winds results in a positive wind stress curl anomaly north of the wind stress maximum, which corresponds to the latitudes of the western boundary (Figure 3.12). This results in an increase in the Ekman pumping (downwelling), which in turn generates downwelling waves against the topographic boundary. As the anomalous wind stress curl in the latitudes of the boundaries is also opposite between $\tau_x^{+50\%}$ and $\tau_x^{-50\%}$, this explains the opposite sign of the waves between these experiments.

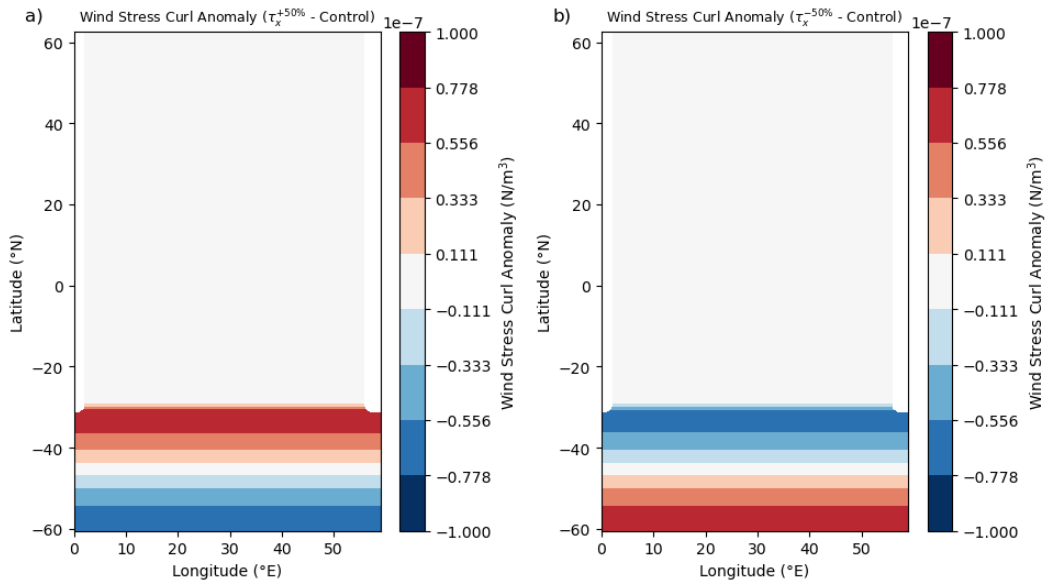

Figure 3.12: Wind stress curl anomalies relative to the control for $\tau_x^{+50\%}$ (a) and $\tau_x^{-50\%}$ (b).

3.4 Mixed Layer Depth Response

One suggested mechanism for enhancing the overturning following a wind forcing is enhanced vertical mixing through a deepening of the mixed layer (Webb *et al.*, 2021). Regardless of whether or not this enhancement of the mixing in the North Atlantic is driving the restructuring of the AMOC itself, a change in the northern deep convection is expected, as to produce additional deep water if greater upwelling is occurring in the south. Webb et al. (2021) found that the mixed layer depth increases in the years following an increase in Southern Ocean wind stress, and that both the downwelling and upwelling modes in their two experiments are capable of deepening the mixed layer, albeit through different pathways. Here I analyse the response of the mixed layer depth for $\tau_x^{+50\%}$ and $\tau_x^{-50\%}$.

Taking a simple proxy of the mixed layer as the depth at which the temperature becomes 0.2°C colder than the surface, the time evolution of the total MLD volumes are plotted for the Northern Hemisphere (Figure 3.13). We can see that indeed, there is a positive relationship between the Southern Ocean winds and the total mixed layer volume. Within the first year the experiments begin to diverge and continue to develop steadily over the 50 years of the experiments. After 50 years, the total North Atlantic mixed layer volume is increased by approximately 3.2% relative to the control in the $\tau_x^{+50\%}$ experiment, and decreased by approximately 6.3% in the $\tau_x^{-50\%}$ experiment. This greater response in $\tau_x^{-50\%}$ seems to be simply due to the volume not yet being in equilibrium, as evidenced by the downward trend in the control.

The geographical distribution of the MLD anomalies is shown through the annually averaged anomalies in Figure 3.14. The changes in the MLD are almost exclusively located above 40°N for both $\tau_x^{-50\%}$ and $\tau_x^{+50\%}$, with the strongest changes in the MLD occurring in the high latitude convective regions above 55°N. Apart from some small patches, the $\tau_x^{+50\%}$ experiments shows a consistent deepening of the ML across the North Atlantic, and $\tau_x^{-50\%}$ shows a consistent shallowing of the ML.

The two experiments in Webb et al. (Webb *et al.*, 2021), despite both increasing the strength of the Southern Ocean winds, generate signals of opposite sign due to the relative locations of the wind stress maxima. Despite one being a

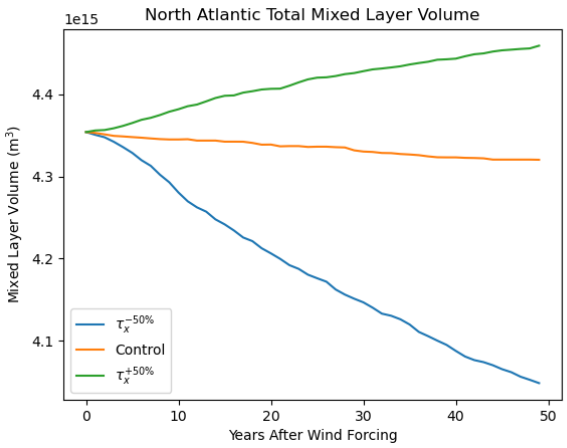

Figure 3.13: Total North Atlantic mixed layer volume for the two wind experiments ($\tau_x^{+50\%}$ in green and $\tau_x^{-50\%}$ in blue) and the control (orange).

downwelling signal, and the other being an upwelling signal, both are seen to deepen the ML upon reaching the North Atlantic. They explain that this is accomplished by differences in the ways that these two signals propagate. In their $\tau^{+15\%}$, downwelling Rossby waves are radiated out from the western boundary in the North Atlantic, depressing isopycnals and deepening the mixed layer, which is also the process that seems to be occurring in this case. On the other hand, in their $\tau_{4^\circ S}^{+15\%}$ experiment, where the winds are shifted southwards, an upwelling signal is generated. This also supports a deepening of the mixed layer by instead traveling along topographic features as a topographic coastal rapped wave hybrid at depth, which upwells denser waters towards the surface, thus increasing mixing. In the case of $\tau_x^{-50\%}$ and $\tau_x^{+50\%}$, they also generate signals of opposite sign, however they both propagate in an identical way, with both of them influencing the mixed layer through the propagation of Rossby waves into the interior. Because the opposite signs of these Rossby waves, they simply have a symmetrical influence on the MLD. In this case, due to the solid boundary across the north, the downwelling/upwelling boundary modes also likely have an influence on this process

Overall, there is indeed a measurable influence on the depth of the mixed layer in the North Atlantic from the Southern Ocean winds. However, as seen earlier in Figure 3.4, the response in the AMOC is clearly originating from the forcing region. Therefore, these changes in the northern convective regions are likely just a response to what is occurring elsewhere in Atlantic, as suggested in Toggweiler and Samuels (1995).

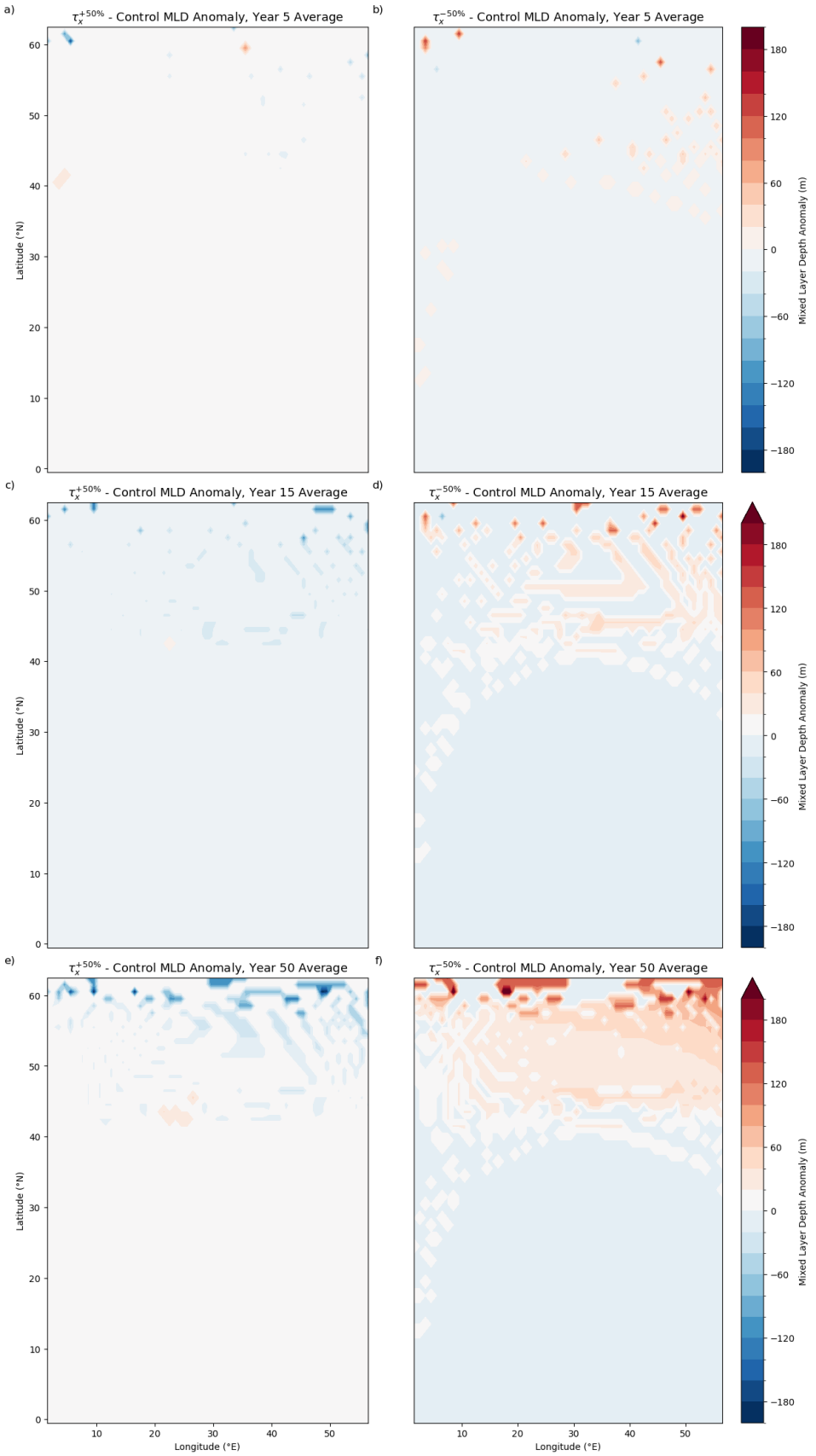

Figure 3.14: Annually averaged Northern Hemisphere MLD anomalies for $\tau_x^{-50\%}$ (b, d, f) and $\tau_x^{+50\%}$ (a, c, e) for 5, 15 and 50 years after the wind forcing.

3.5 Upwelling Structure

In Section 3.2, the zonally averaged overturning streamfunction told us little about the horizontal structure of the AMOC. If we wish to more closely examine how the AMOC is restructuring following the wind forcing, we need to examine different variables. Here, I consider the vertical velocity (w) and corresponding volume transport and observe how the upwelling/downwelling evolves over time, as well as how these changes relate to the signals identified in Section 3.3.

At the end of the spinup period, the vertical transport field averaged over the final year at 782.4m is shown in Figure 3.15. This depth is chosen to analyse as this corresponds the depth of the maximum overturning strength of the upper NADW cell (Figure 3.1). According to the classical Stommel-Arons theory of abyssal circulation, localised areas of sinking should be compensated by widespread upwelling spread throughout the ocean interior (Stommel and Arons, 1959b). Here, we see an ocean where the downwelling regions are indeed localised, as expected. The downwelling regions are primarily located along the northern boundary and at the north-eastern corner of the model domain corresponding to the regions of NADW formation (Figure 3.1). Most of the interior shows a weak upwelling, matching the Stommel-Arons theory, however there are large patches in the north-west interior that instead show a downward transport. This interior downwelling is primarily located adjacent to the western boundary, and is likely partially compensating for the very large upwelling there.

The upwelling on the other hand is less similar to expectations. Especially obvious here is the abnormally large upwelling taking place in the final grid cell at the western boundary, with 12.68Sv compared to 3.37Sv for the entire interior of the North Atlantic (Figure 3.15). The degree to which the western boundary is dominant compared to the interior appears to be dependant on latitude, where at the higher latitudes the upwelling becomes more concentrated at the western boundary (Figure 3.16). Having such large values of upwelling concentrated at the boundaries is a known phenomenon with coarse resolution models. This could be due to the fact that the Rossby radius of deformation is not resolved at such resolutions, meaning these sub-grid scale processes must be parameterised, which can result in unrealistic values under

certain schemes (Huck *et al.*, 1999). The Rossby radius also gets smaller with increasing latitude, which could explain why this effect appears larger at the high latitudes. It does also seem that this effect is less pronounced in the Southern Hemisphere, but is still present (Figure 3.16a)

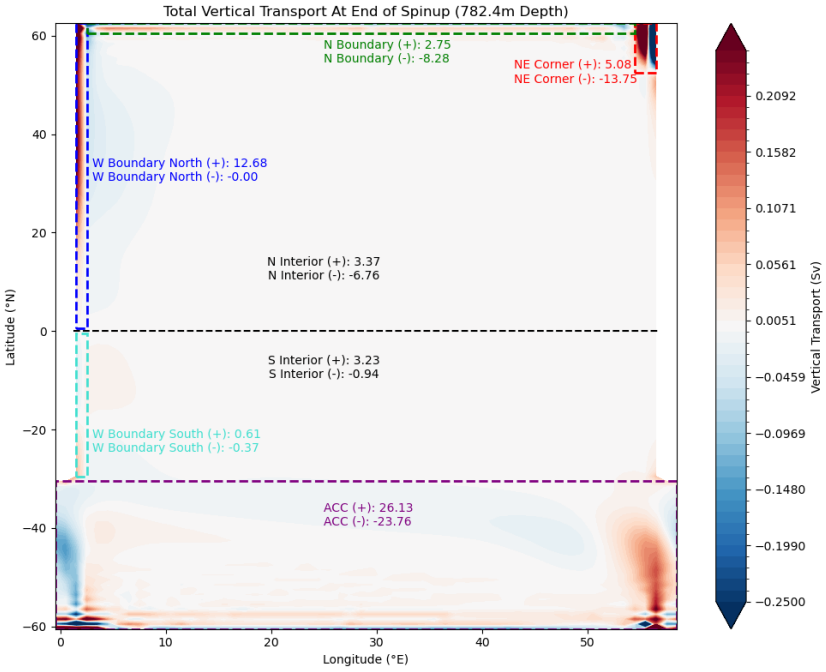

Figure 3.15: Vertical transport (Sv) at 782.4m depth at the end of the spinup period. The coloured rectangles separate the totals for regions where the vertical transport is particularly high. The numbers displayed show the total amount of upwards transport (+) and downwards transport (-) for each region. The interior is simply defined as the regions not belonging to those delineated by the coloured rectangles, split between the northern and southern hemispheres.

To observe how the upwelling is changing following the wind forcing, we can consider the anomaly in the vertical transport. The annually averaged vertical velocity field anomaly at 782.4m depth is shown in Figure 3.17 for the two experiments. In terms of the NADW formation, a response is seen in both $\tau_x^{+50\%}$ and $\tau_x^{+50\%}$, as there is an increase in the total downwelling in the northern convective regions which develops over the 50 year period. The upwelling in the western boundary is also affected, although this does not develop significantly until a few years after the forcing. The size of the anomaly in the western boundary upwelling is also quite small relative to the absolute values here. After 50 years, the total vertical transport in the western boundary sees a 5% increase in $\tau_x^{+50\%}$ and a 4.9% decrease in $\tau_x^{-50\%}$.

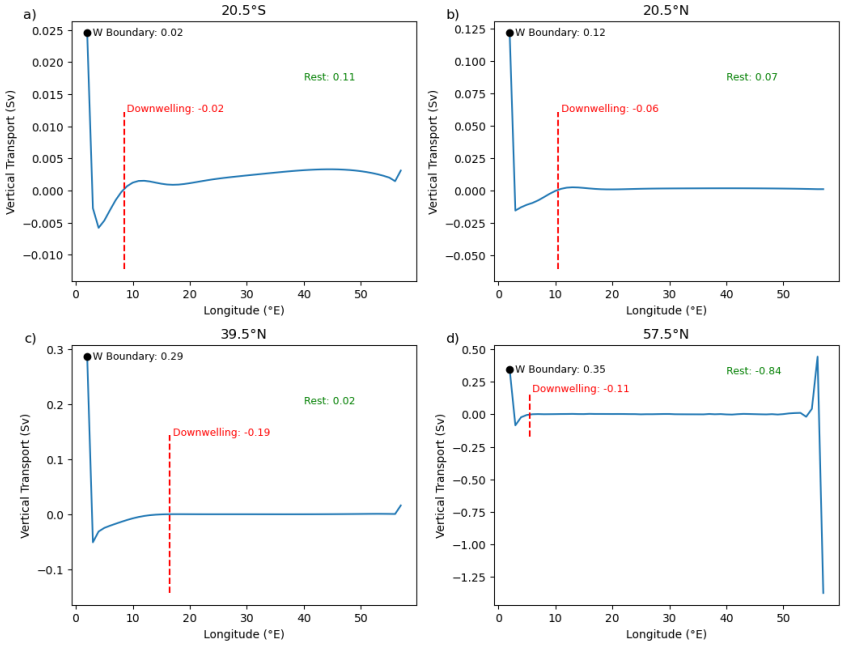

Figure 3.16: Vertical transport (Sv) at 782.4m depth at the end of the spinup period for 4 different latitude cuts. The black dot indicates the final grid cell at the western boundary. The red dotted line shows where the downwelling region adjacent to the western boundary ends, with the corresponding red text showing the vertical transport summed over this region. The green text indicates sum of the vertical transport to the right of the red dotted line.

We can see that although the boundaries were evidently dominant in absolute terms when considering the vertical transport at the end of the spinup period, the largest anomaly is instead in the interior. It is also notable that the interior upwelling actually has an inverse relationship with the strength of the Southern Ocean winds, which is particularly visible in the interior of the South Atlantic. After 50 years in $\tau_x^{+50\%}$, there is a 1.15Sv reduction in the vertical transport in the southern hemisphere interior, whereas $\tau_x^{-50\%}$ sees a 1.20Sv increase. A possible reason for this inverse relationship is that when the strength of the winds in the Southern Ocean are increased, the role of the Southern Ocean upwelling could become more important in the overall upwelling structure. In the Stommel-Arons view of the abyssal circulation, the interior diapycnal mixing brings the deep water into the thermocline, however as explained in Toggweiler and Samuels (Toggweiler and Samuels, 1995), deep water can also be brought to the surface through movement along isopycnals which outcrop in the ACC. Therefore, it appears here that when increasing the wind stress in the Southern Ocean, more water is upwelled in the ACC instead of the interior. This is also consistent with the fact that the only region which sees an

increase in the vertical transport of a similar amount, and of opposite sign to the interior is in the ACC vertical transport anomalies. This would also explain the pattern in the zonally averaged overturning anomaly (Figure 3.4), where by following the streamlines, the anomalous overturning circulation can be seen to be almost entirely be circulating poleward beneath the depth of the sill, and being upwelled in the ACC.

Figure 3.18 shows the time evolution of the total vertical transport for the delineated regions for the first 15 years. This can give us some idea of the relevant signals in the restructuring process. At the northern boundary (3.18d), the downwelling is enhanced in $\tau_x^{+50\%}$ and decreased in $\tau_x^{-50\%}$ relative to the control, and begins to diverge after approximately 100 days, which aligns with the arrival of the boundary modes in this region. At the western boundary, the experiments take much longer to depart from the control in comparison, with the two experiments being approximately equal until about 1000 days after the wind forcing. Westward propagating Rossby modes have been implicated in the adjustment of the western boundary current in other studies (McDermott, 1996, Marshall and Johnson, 2013), and this timing does align with when the Rossby modes at the low latitudes begin to arrive at the western boundary (Figure 1.4). For the interior of the South Atlantic and the ACC, the vertical transport seems to already experience significant adjustment in just the first day, which is expected given this is where the forcing is occurring. These time evolution plots also make it apparent that the vertical transports in some of these regions are not in equilibrium, and therefore could continue to develop and become more important in the adjustment of the overturning on longer time scales.

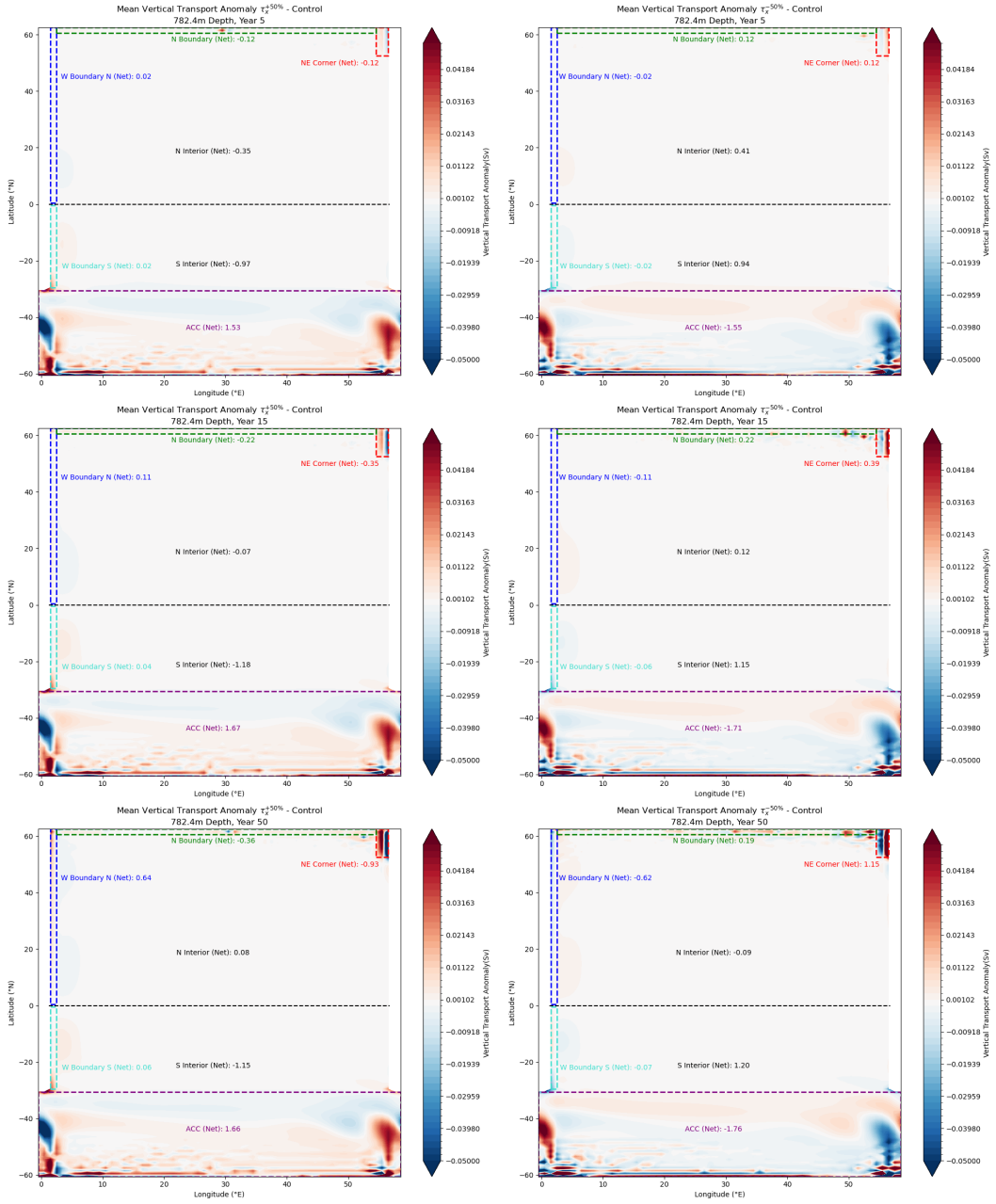

Figure 3.17: Annual averages of the vertical transport anomaly for 3 different years at 782.4m depth for $\tau_x^{-50\%}$ (a, c, e) and $\tau_x^{-50\%}$ (b, d, f), each relative to the control. Interior values are excluding the delineated regions.

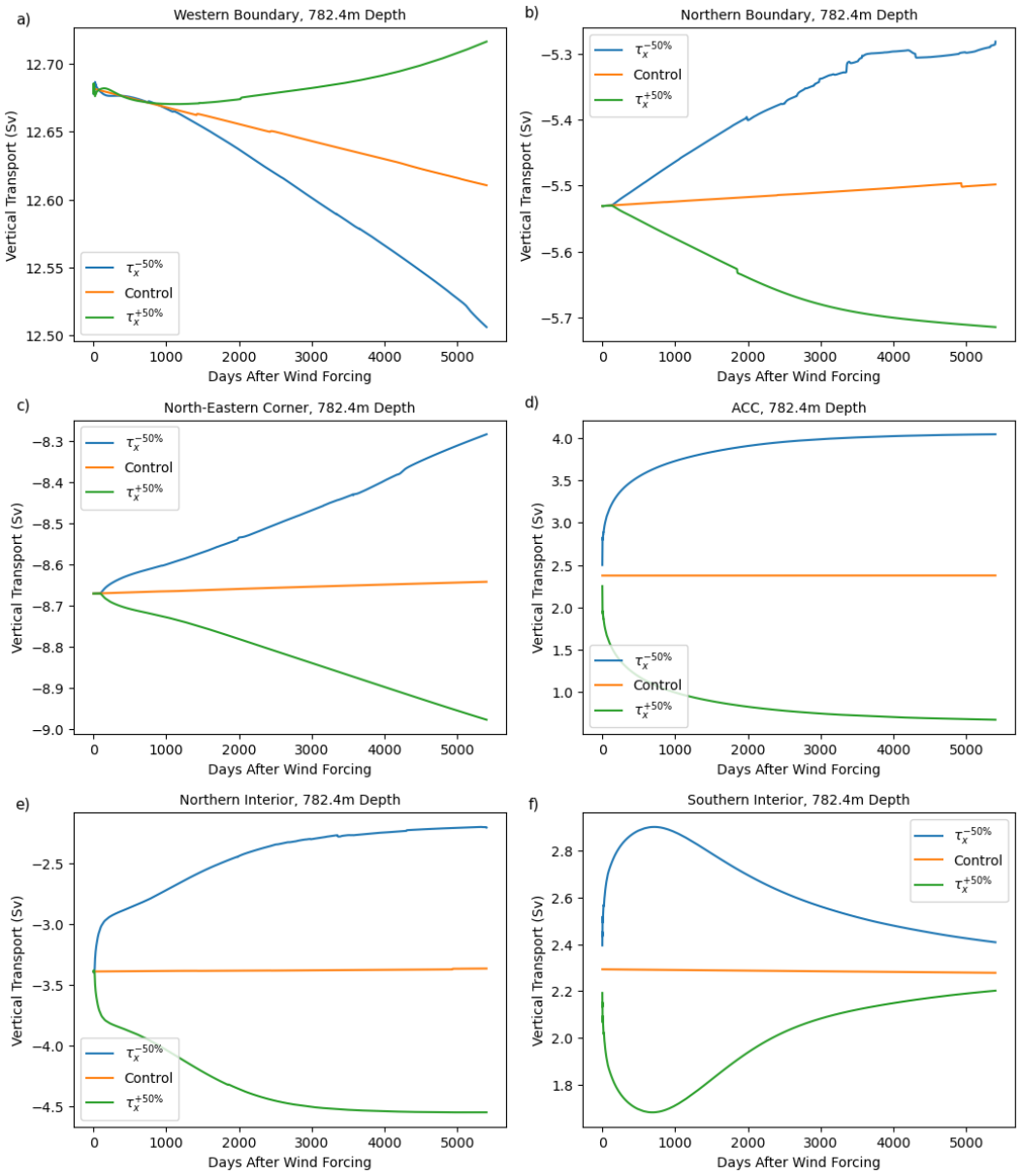

Figure 3.18: Evolution of the total vertical transport for $\tau_x^{-50\%}$ (blue), $\tau_x^{+50\%}$ (green), and the control (orange) over the first 15 years of the experiment for 6 different regions. These regions correspond to those marked out in Figure 3.15

.

4 Summary and Discussion

This thesis was originally motivated by McDermott (1996), where these baroclinic boundary and Rossby waves were identified as the link between a wind forcing in Southern Ocean, and the North Atlantic deep convection. McDermott describes the path and nature of these signals, but stops short of explaining how these waves enhance convection in the North Atlantic. My aim was to expand upon this by exploring how these signals cause changes upon reaching the areas of NADW formation, and how the overall structure of the AMOC adjusts in response. To do this I set up two experiments $\tau_x^{+50\%}$ and $\tau_x^{-50\%}$ which modified the strength of the winds in the latitudes of a re-entrant channel in an idealised model of the Atlantic Ocean.

First, I wanted to verify that there was indeed a 'Drake Passage Effect' in this model and setup. For both experiments, I found a clear sensitivity of the maximum overturning strength to wind forcings in the channel, where the amplitude of the Southern Ocean winds had a positive correlation with the strength of the overturning. There was found to be quite a large sensitivity in the overturning strength as measured in the South Atlantic, and a lower, but still present sensitivity in the north. Following the wind forcing, the anomalous overturning was seen to begin in the forcing region, and migrate northwards, with the strongest anomalies seen in the South Atlantic. Questions of course still remain about whether this sensitivity is realistic, given the coarse resolution, and lack of variable eddy parameterisation (Gent, 2016). However, this was not the focus of this thesis, but instead, the fact that there is a connection was enough to proceed.

As described in McDermott (1996), the wind forcing in the channel excites waves at the western boundary of the South Atlantic. These waves travels as kelvin-like baroclinic modes along the western boundary, before turning and following along the equator. Upon reaching the eastern boundary of the domain, it divides symmetrically, travelling both north and south. As this mode travels along the eastern boundary of the model domain, it radiates out first-mode baroclinic Rossby waves, which carry the signal westward into the ocean

interior. The boundary mode turns and continues along the northern boundary, with the maximum of the anomaly shifting down to approximately 2500m depth as a result of the significant change in stratification. This behaviour is not described by other papers investigating this topic. McDermott (1996) simply states that this signal 'locks on' to pre-existing sinking regions in the north-eastern corner of the model domain and enhances the convection there. The signal is likely then able to continue influence the convection along the northern boundary, instead of only enhancing the convection in the north-eastern corner.

Upon reaching the north, the signal must induce some kind of change in these regions to enhance the deep convection. In Webb et al. (2021), this change was a deepening of the mixed layer, enhancing the total mixing in these regions. This was also observed in these experiments, as there was a clear response in the mixed layer depth coinciding with the arrival of the wave signals following the forcing. This response is largely symmetrical between $\tau_x^{+50\%}$ and $\tau_x^{-50\%}$, where the total mixed layer depth increases in the case of stronger winds, and decreases with weaker winds. Where the findings in this thesis differ however, is that the changes in the North Atlantic do not appear to be dominant in the overall restructuring of the AMOC.

As was discussed in the introduction, there are broadly two different ways that the AMOC is seen to respond to Southern Ocean wind forcing in other studies. The first being that the changes in the Ekman transport and corresponding deep poleward return flow causes changes in the zonally averaged overturning to migrate northward i.e. Toggweiler and Samuels (1995) and the $\tau^{+15\%}$ case in Webb et al. (2021). The other pattern found is that corresponding changes in the North Atlantic occur first, and then migrate back towards the forcing region i.e. McDermott (1996) and the $\tau_{4^\circ S}^{+15\%}$ case in Webb et al. (2021). In these experiments, it is the former process that is observed.

The analysis of the upwelling structure revealed that that largest changes in the vertical transport were taking place in the interior of the South Atlantic and the ACC. In $\tau_x^{+50\%}$, there was found to be greater downwelling in the Northern convective regions following the forcing, while also a decrease in upwelling in the interior. The largest increases in the upwelling where found to instead be taking place in the ACC. In $\tau_x^{-50\%}$, on the other hand, the opposite response is

simply seen, with reduced downwelling in the NADW formation regions, and increased upwelling in the interior as opposed to the ACC.

Overall, these upwelling results combined with the zonally averaged overturning results points toward an adjustment process dominated by a sort of 'spill-over' from the ACC following the wind forcing. As the winds are increased, a greater volume of water is moved northward at the surface via Ekman transport. The greater winds also impart more energy in the ACC, which is stored in the form of potential energy by tilting of density surfaces (Marshall and Speer, 2012). This causes water that would have otherwise been upwelling into the thermocline via diapycnal mixing is instead diverted along isopycnals and towards the ACC. As mentioned in Section 1.3, this more closely matches the process described in Toggweiler and Samuels (1995), where the NADW formation enhancement is just simply closing the large scale circulation initiated in the south. This change therefore slowly migrates northward, as the density structure of the ocean is steadily adjusted to account for these changes in the dynamics of the Southern Ocean.

A potential issue with the experimental design here is that the wind stress profile applied has a zero-crossing point precisely at 30°S (Figure 2.2), meaning that when the forcing is applied, there is actually no wind stress curl anomaly against the topographical boundaries. This is undesirable when the goal is to generate a signal, and could have resulted in a weaker signal than otherwise expected. While this would not influence the changes in the Ekman transport in the Southern Ocean, it may have implications for the changes in the north, which are induced by the arrival of the signal. Whether this would have resulted in a different adjustment process is unclear, but important to acknowledge.

The broader applicability of the results from the experiments performed in this thesis are also limited by the simplicity of the model. With a relatively coarse resolution of just one degree, idealised topography, and just a single basin, the model domain clearly does not resemble the real ocean, and is unable to support or resolve certain processes that could be relevant. For instance, in $\tau_x^{-50\%}$ in the upwelling structure results it was shown that the interior upwelling increased following the wind forcing, which I hypothesised was due to the fact that this was water that would otherwise have been upwelling in the ACC. However, in a global GCM it has been suggested that a reduction of

the Southern Ocean winds can result in increased upwelling in other oceans, and that this need not necessarily impact the overturning in the North Atlantic (Jochum and Eden, 2015). This kind of process is not able to occur in just a single basin. Another important feature of the ocean that is not represented in this model is topographic features on the ocean floor. There is evidence that diapycnal mixing in the ocean is highly non-uniform, and that due to bottom topography, certain regions experience much higher turbulent mixing as a result of the breaking of internal waves over rough surfaces (Ledwell *et al.*, 2000). With just a simple flat bottom in these experiments, there is no topography to enhance the diapycnal mixing, and therefore this component of the overturning could be underestimated.

This is of course, not to discount the results of the humble box model. Through the simplifications, perhaps some of the processes highlighted in this thesis are made clearer, which can serve as a starting point for more detailed analyses. Additionally, many global climate models are also run at relatively coarse resolutions of approximately 1 degree, meaning it is still very relevant to understand how these processes are represented at coarser resolutions.

Future Work

5

This thesis explored a number of different aspects of the AMOC adjustment process, and therefore there are naturally a few ways that some of this work could be extended. Some avenues include:

- Further investigation of the nature of the boundary modes. Can they be identified as classical Kelvin waves? Or instead as the short/long Rossby waves as suggested by Marshall and Johnson (2013). This could be tested by adjusting model resolution and boundary layer parameters.

- In the experiments, it seemed that the strength of the winds resulted in NADW being upwelled either in the ACC or in the interior at differing proportions. Tracer experiments could follow the path of this water and compare between different wind forcings to confirm where the additional NADW is moving.

- Refining the wind stress profile and model topography. In these experiments. This would result in a greater area where the wind stress curl anomaly is in contact with the topographic boundaries. This could result in a stronger signal, and therefore change the manner in which the ocean responds.

- Investigation of the downward shift of the signal at the northern convective regions. What is the precise nature of the processes here? What implications does this have for the response of the AMOC?

Bibliography

6

Alley, R B, J Marotzke, W D Nordhaus, *et al.* (2003). “Abrupt Climate Change”. en. In: 299.

Andreasen, Laurits S (2020). “Time scales of the Bipolar seesaw: The role of oceanic cross-hemisphere signals, Southern Ocean eddies and wind changes”. MA thesis. University of Copenhagen.

Buckley, Martha W. and John Marshall (Mar. 2016). “Observations, inferences, and mechanisms of the Atlantic Meridional Overturning Circulation: A review”. en. In: *Reviews of Geophysics* 54.1, pp. 5–63.

Chelton, Dudley B., Roland A. deSzoeke, Michael G. Schlax, Karim El Naggar, and Nicolas Siwertz (Mar. 1998). “Geographical Variability of the First Baroclinic Rossby Radius of Deformation”. en. In: *Journal of Physical Oceanography* 28.3, pp. 433–460.

Deng, Kaiqiang, Cesar Azorin-Molina, Song Yang, Chundi Hu, Gangfeng Zhang, Lorenzo Minola, and Deliang Chen (June 2022). “Changes of Southern Hemisphere westerlies in the future warming climate”. en. In: *Atmospheric Research* 270, p. 106040.

Gent, Peter R. (Jan. 2016). “Effects of Southern Hemisphere Wind Changes on the Meridional Overturning Circulation in Ocean Models”. en. In: *Annual Review of Marine Science* 8.1, pp. 79–94.

Greatbatch, Richard J. and K. Andrew Peterson (Sept. 1996). “Interdecadal variability and oceanic thermohaline adjustment”. en. In: *Journal of Geophysical Research: Oceans* 101.C9, pp. 20467–20482.

Häfner, Dion, René Løwe Jacobsen, Carsten Eden, Mads R. B. Kristensen, Markus Jochum, Roman Nuterman, and Brian Vinter (Aug. 2018). “Veros v0.1 – a fast and versatile ocean simulator in pure Python”. en. In: *Geoscientific Model Development* 11.8, pp. 3299–3312.

Hansen, Rasmus Ranum (2023). “Solving the turbulence closure problem II”. MA thesis. University of Copenhagen.

Huck, Thierry, Andrew J. Weaver, and Alain Colin De Verdière (May 1999). “On the influence of the parameterization of lateral boundary layers on the thermohaline circulation in coarse-resolution ocean models”. en. In: *Journal of Marine Research* 57.3, pp. 387–426.

Jochum, M. and Carsten Eden (Dec. 2015). “The Connection between Southern Ocean Winds, the Atlantic Meridional Overturning Circulation, and Indo-Pacific Upwelling”. en. In: *Journal of Climate* 28.23, pp. 9250–9257.

Kawase, Mitsuhiro (Dec. 1987). “Establishment of Deep Ocean Circulation Driven by Deep-Water Production”. en. In: *Journal of Physical Oceanography* 17.12, pp. 2294–2317.

Kuhlbrodt, T., A. Griesel, M. Montoya, A. Levermann, M. Hofmann, and S. Rahmstorf (June 2007). “On the driving processes of the Atlantic meridional overturning circulation”. en. In: *Reviews of Geophysics* 45.2, 2004RG000166.

Kunze, Eric, Eric Firing, Julia M Hummon, Teresa K Chereskin, and Andreas M Thurnherr (2006). “Global Abyssal Mixing Inferred from Lowered ADCP Shear and CTD Strain Profiles”. en. In: *JOURNAL OF PHYSICAL OCEANOGRAPHY* 36.

Ledwell, J R, L C St Laurent, J B Girton, and J M Toole (2011). “Diapycnal Mixing in the Antarctic Circumpolar Current”. en. In: *JOURNAL OF PHYSICAL OCEANOGRAPHY* 41.

Ledwell, J. R., E. T. Montgomery, K. L. Polzin, L. C. St. Laurent, R. W. Schmitt, and J. M. Toole (Jan. 2000). “Evidence for enhanced mixing over rough topography in the abyssal ocean”. en. In: *Nature* 403.6766, pp. 179–182.

Marshall, David P. and Helen L. Johnson (Dec. 2013). “Propagation of Meridional Circulation Anomalies along Western and Eastern Boundaries”. en. In: *Journal of Physical Oceanography* 43.12, pp. 2699–2717.

Marshall, John and Kevin Speer (Mar. 2012). “Closure of the meridional overturning circulation through Southern Ocean upwelling”. en. In: *Nature Geoscience* 5.3, pp. 171–180.

McDermott, David A. (July 1996). “The Regulation of Northern Overturning by Southern Hemisphere Winds”. en. In: *Journal of Physical Oceanography* 26.7, pp. 1234–1255.

Munk, Walter and Carl Wunsch (Dec. 1998). “Abyssal recipes II: energetics of tidal and wind mixing”. en. In: *Deep Sea Research Part I: Oceanographic Research Papers* 45.12, pp. 1977–2010.

Osychny, Vladimir and Peter Cornillon (Jan. 2004). “Properties of Rossby Waves in the North Atlantic Estimated from Satellite Data”. en. In: *Journal of Physical Oceanography* 34.1, pp. 61–76.

St. Laurent, Louis and Chris Garrett (Oct. 2002). “The Role of Internal Tides in Mixing the Deep Ocean”. en. In: *Journal of Physical Oceanography* 32.10, pp. 2882–2899.

Stommel, Henry (May 1961). “Thermohaline Convection with Two Stable Regimes of Flow”. en. In: *Tellus* 13.2, pp. 224–230.

Stommel, Henry, A. B. Arons, and A. J. Faller (May 1958). “Some Examples of Stationary Planetary Flow Patterns in Bounded Basins”. en. In: *Tellus* 10.2, pp. 179–187.

Stommel, Henry and A.B. Arons (Jan. 1959a). “On the abyssal circulation of the world ocean—I. Stationary planetary flow patterns on a sphere”. en. In: *Deep Sea Research (1953)* 6, pp. 140–154.

Stommel, Henry and A.B. Arons (1959b). “On the abyssal circulation of the world ocean—II. An idealized model of the circulation pattern and amplitude in oceanic basins”. en. In: *Deep Sea Research* 6, pp. 217–233.

Toggweiler, J. R. (Mar. 2009). “Shifting Westerlies”. en. In: *Science* 323.5920, pp. 1434–1435.

Toggweiler, J.R. and B. Samuels (Apr. 1995). “Effect of drake passage on the global thermohaline circulation”. en. In: *Deep Sea Research Part I: Oceanographic Research Papers* 42.4, pp. 477–500.

Toole, John M., Raymond W. Schmitt, and Kurt L. Polzin (May 1994). “Estimates of Diapycnal Mixing in the Abyssal Ocean”. en. In: *Science* 264.5162, pp. 1120–1123.

Vallis, Geoffrey K. (2017). *Atmospheric and Oceanic Fluid Dynamics*. Cambridge University Press.

Wajsowicz, Roxana C. (Dec. 1986). “Adjustment of the Ocean under Buoyancy Forces. Part II: The Role of Planetary Waves”. en. In: *Journal of Physical Oceanography* 16.12, pp. 2115–2136.

Wajsowicz, Roxana C. and A. E. Gill (Dec. 1986). “Adjustment of the Ocean under Buoyancy Forces. Part I: The Role of Kelvin Waves”. en. In: *Journal of Physical Oceanography* 16.12, pp. 2097–2114.

Wang, Wei and Rui Xin Huang (Sept. 2005). “An experimental study on thermal circulation driven by horizontal differential heating”. en. In: *Journal of Fluid Mechanics* 540.-1, p. 49.

Webb, D. J., P. Spence, R. M. Holmes, and M. H. England (May 2021). “Planetary-wave induced strengthening of the AMOC forced by poleward intensified Southern Hemisphere westerly winds”. en. In: *Journal of Climate*, pp. 1–45.